

Structure-Aware Matrix Pencil Method

Yehonatan-Itay Segman, Alon Amar, and Ronen Talmon, *Senior Member, IEEE*

Abstract—We address the problem of detecting the number of complex exponentials and estimating their parameters from a noisy signal using the Matrix Pencil (MP) method. We introduce the MP *modes* and present their informative spectral structure. We show theoretically that these modes can be divided into signal and noise modes, where the signal modes exhibit a perturbed Vandermonde structure. Leveraging this structure, we propose a new MP algorithm, termed the SAMP algorithm, which has two novel components: (i) a robust, theoretically grounded model-order detection method, and (ii) an efficient estimation of the signal amplitudes. We show empirically that SAMP significantly outperforms the standard MP method in challenging conditions, with closely-spaced frequencies and low Signal-to-Noise Ratio (SNR) values, approaching the Cramer-Rao lower bound (CRB) for a broad SNR range. Additionally, compared with prevalent information-based criteria, we show that SAMP achieves comparable or better results with lower computational time, and lower sensitivity to noise model mismatch.

Index Terms—Matrix Pencil Method, model order detection, Parameter estimation, closely-spaced frequencies, super-resolution.

I. INTRODUCTION

CONSIDER the classical model of a discrete-time signal consisting of a sum of complex exponentials and additive noise:

$$y(n) = x(n) + w(n), \quad (1)$$

where $0 \leq n \leq N - 1$, $w(n)$ is the additive noise, and $x(n)$ is the signal term expressed as a finite sum of complex exponentials given by:

$$x(n) = \sum_{i=1}^M b_i e^{(-\alpha_i + j\theta_i)n}, \quad (2)$$

where M is the number of complex exponentials (or model order), $b_i = |b_i|e^{j\phi_i}$ are the complex amplitudes, $\phi_i \in \mathbb{R}$ are the initial phases, $\alpha_i \in \mathbb{R}$ are the (non-negative) damping factors, $\theta_i \in \mathbb{R}$ are the normalized frequencies, and the lower case letter ‘j’ is the complex number $j = \sqrt{-1}$. The complex exponentials $e^{-\alpha_i + j\theta_i}$ are conventionally represented as $z_i = e^{-\alpha_i + j\theta_i}$, and referred to as the signal poles. The signal poles are assumed to be distinct. Given the finite interval of N samples of $y(n)$, the goal is twofold: (i) detect the (discrete-valued) model order M (a detection step), and (ii) determine the (continuous-valued) parameters of interest (an estimation step), i.e., $\{b_i\}_{i=1}^M$, $\{\alpha_i\}_{i=1}^M$, and $\{\theta_i\}_{i=1}^M$.

This is a longstanding fundamental detection-estimation problem in signal processing, with a broad variety of applications in telecommunications, audio processing, radar systems, and biomedical signal analysis [1–3]. Over the years,

The authors are with the Viterbi Faculty of Electrical and Computer Engineering, Technion – Israel Institute of Technology, Haifa 32000, Israel. Corresponding author: Yehonatan-Itay Segman, email: yehonatans@campus.technion.ac.il.

numerous methods have been proposed, including maximum likelihood-based techniques [4–6], super-resolution pseudospectrum approaches such as Minimum Variance Distortionless Response (MVDR) (known also as Capon’s method) [7], MULTiple SIgnal Classification (MUSIC) [8], Estimation of Signal Parameters via Rotational Invariant Techniques (ESPRIT) [9], Method Of Direction Estimation (MODE) [10], SParse Iterative Covariance-based Estimation (SPICE) [11], sparse model-based methods [12–18], optimization-based techniques [19, 20], and more recently, neural network-based approaches [21–27].

One common approach for such problems is based on information measures such as the Akaike Information Criterion (AIC), Bayesian Information Criterion (BIC), or Minimum Description Length (MDL) [1, 3]. In this approach, the detection and estimation steps are *coupled*; for each hypothesized model order, the most likely parameters are estimated. Despite its popularity and widespread use, this coupled approach has two main drawbacks. (i) It necessitates the computation of the likelihood function, which is usually unknown in practice. (ii) It is computationally demanding, as it involves repeated model parameter estimations for each hypothesized model order.

More computationally efficient is a *decoupled detection and estimation* approach, where the model order is determined first, followed by parameter estimation. A common *non-parametric* method involves computing a spectrum (or pseudo-spectrum) of the observations. For example, the model order can be determined by counting the number of significant peaks in the periodogram (or even Bartlett’s or Welch’s spectrum). This efficiency comes at the expense of two prominent limitations: limited frequency resolution, which is proportional to the reciprocal of the data length, and tapering / windowing effects [28]. These limitations pose significant concerns for short time series, and many alternatives have been proposed to mitigate them.

Herein, we consider the *decoupled detection and estimation* approach and focus on the MP method, introduced by Hua and Sarkar in [29], as a super-resolution method. The MP method estimates the frequencies of superimposed complex exponentials by solving a generalized eigenvalue problem derived from the signal’s Hankel matrix. Consequently, compared to the classical Fourier analysis, it is not restricted to a specific regular grid and does not have a separation limit due to tapering. The MP method has gained considerable attention for its superiority over other linear methods, such as Prony-based methods, demonstrating robustness to noise and computational efficiency [30, 31].

Several modifications to the MP algorithm that mitigate its sensitivity to additive white noise have been proposed in the literature including the Forward-Backward MP (FBMP) approach [30, 31] which is limited to undamped exponentials,

the Band-Pass MP (BPMP), which is effective in the case of damped exponentials though its implementation requires prior knowledge of the signal and increased computation time [32], the Total-Least-Squares MP (TLS-MP) approach, which uses a pre-filtering step for noise mitigation [31], and the Total Forward-Backward MP (TFBMP), which surpasses the Fast Fourier Transform (FFT) in variance estimates beyond a specific SNR threshold, at the expense of a larger bias [33].

The above variations of the MP method first determine the model order of the problem through singular values truncation, then estimate the poles from the generalized eigenvalues, and finally estimate the amplitudes by solving a linear least square problem [31]. Additionally, the main theoretical result, introduced in [29, Theorem 2.1], only addresses noiseless scenarios, whereas noise is almost always present in real-world applications. The discrepancy between the ideal noiseless scenario in theory and the presence of noise in practice highlights the need to extend the MP theory to handle noisy signals.

In this paper, we present a new MP method, termed the Structure-Aware Matrix Pencil (SAMP), which implements a new strategy of “first estimate and then detect”, rather than the standard “detect and then estimate” approach. Our new method has two novel components: (i) a new approach for model order detection, and (ii) an efficient amplitude estimation. At the core of our method lie the MP *modes*, a new notion that is borrowed from the realm of dynamic mode decomposition (DMD) [34] and introduced in this context for the first time to the best of our knowledge. Concretely, the left and right MP *modes* are defined as the columns and rows of the pseudo-inverse matrix of the generalized eigenvectors matrix obtained by the MP method, respectively.

We show theoretically that these MP modes can be divided into signal modes and noise modes, where the signal modes exhibit a perturbed Vandermonde structure. We theoretically study this perturbation and explicitly present the dependency on the model parameters. We put special focus on the impact of noise and extend the classical MP theorem in [29] to address noisy scenarios and demonstrate that all the signal components in (2) can be detected through the signal modes. Leveraging the structure of the signal modes, we depart from singular values thresholding heuristics. Instead, we propose a new model order detection with theoretical guarantees that depend on the SNR and the separation of the poles. We show empirically that the new SAMP algorithm obtains superior performance compared with the standard MP method that is based on singular values thresholding for the model order detection, particularly in challenging conditions with closely-spaced frequencies and low SNR values in the threshold region, where model-order estimation becomes challenging. In addition, we show that compared with the prevalent information-based criteria, SAMP is less sensitive to noise model mismatch and is more computationally efficient.

The paper is organized as follows. In Sec. II we describe the existing MP method. In Sec. III we introduce the MP modes and analyze their structure. In Sec. IV we propose a novel order detection rule based on the MP modes structure. In Sec. V we proposed an efficient method for estimating the signal amplitudes using the MP modes. In Sec. VI we present

the SAMP algorithm for estimating the model parameters. In Sec. VII we present simulation results. Finally, in Sec. VII-D we summarize this paper with conclusions and discussion regarding possible practical implications and future research.

II. THE CLASSICAL MATRIX PENCIL METHOD

The MP method estimates signal parameters by solving a generalized eigenvalue problem based on the available data samples. It begins by constructing an $(N - L) \times (L + 1)$ Hankel matrix \mathbf{Y} from the noisy measurements $y(n)$:

$$\mathbf{Y} = \begin{bmatrix} y(0) & y(1) & \cdots & y(L) \\ y(1) & y(2) & \cdots & y(L+1) \\ \vdots & \vdots & \ddots & \vdots \\ y(N-L-1) & y(N-L) & \cdots & y(N-1) \end{bmatrix}. \quad (3)$$

The parameter L , termed the *pencil parameter*, is chosen to satisfy $M \leq L \leq N - M$ (see sec. II-C for more details). Using perturbation analysis, it was demonstrated that the optimal range for minimizing variance in the estimator is $\frac{N}{3} \leq L \leq \frac{N}{2}$ [29, 30, 35–37]. For the rest of this paper, we assume that L lies within this optimal range.

Next, two sub-matrices \mathbf{Y}_0 and \mathbf{Y}_1 are formed from \mathbf{Y} by removing its last and first columns, respectively. A denoising step (see section II-A) is then performed using the singular value decomposition (SVD) of the Hankel matrix \mathbf{Y}_0 :

$$\mathbf{Y}_0 = \mathbf{U}\Sigma\mathbf{V}^H, \quad (4)$$

where $\mathbf{U} \in \mathbb{C}^{(N-L) \times L}$ and $\mathbf{V} \in \mathbb{C}^{L \times L}$ are unitary matrices, $\Sigma = \text{diag}(\sigma_1, \dots, \sigma_L)$ with $\sigma_1 \geq \sigma_2 \geq \dots \geq \sigma_L$, and $(\cdot)^H$ denotes the complex conjugate transpose.

Using (4) we can express the MP by:

$$\mathbf{Y}_1 - \tilde{\lambda}\mathbf{Y}_0 = \mathbf{U}\Sigma(\mathbf{A} - \tilde{\lambda}\mathbf{I})\mathbf{V}^H, \quad (5)$$

where the square, non-symmetric, $L \times L$ matrix \mathbf{A} is given by:

$$\mathbf{A} = \Sigma^{-1}\mathbf{U}^H\mathbf{Y}_1\mathbf{V}, \quad (6)$$

and we use the notation of $\tilde{\lambda}$ to denote a perturbation of λ , an eigenvalue of the noiseless MP (see Section II-C for more details). The MP method is based on finding the eigenvalues of the MP $\mathbf{Y}_1 - \tilde{\lambda}\mathbf{Y}_0$ as an estimate for the signal poles z_i . Instead of directly computing the eigenvalues of $\mathbf{Y}_1 - \tilde{\lambda}\mathbf{Y}_0$, the estimates of the signal poles are obtained by the eigenvalues of \mathbf{A} [29]. Accordingly, an eigenvalue decomposition (EVD) of the matrix \mathbf{A} is performed:

$$\mathbf{A} = \mathbf{Q}\tilde{\Lambda}\mathbf{Q}^{-1}, \quad (7)$$

where $\tilde{\Lambda} = \text{diag}(\tilde{\lambda}_1, \dots, \tilde{\lambda}_L)$ and $\mathbf{Q} \in \mathbb{C}^{L \times L}$ contains the eigenvectors as columns.

A critical problem arises as the matrices \mathbf{Y}_0 and \mathbf{Y}_1 have a full rank (which equals L) stemming from the additive noise contamination. Consequently, the matrix \mathbf{A} has L non-zero eigenvalues, consisting of M signal-related eigenvalues, and $L - M$ extraneous eigenvalues, containing only noise-related information [31]. Therefore, the model order (the number of complex exponentials) needs to be determined in addition to, and usually before, the estimation of the parameters.

A. Model order detection

Determining the model order in the MP method involves truncating the singular values from the SVD of \mathbf{Y}_0 in (4), and the standard approach for this step is the decoupled detection-estimation approach. A commonly used technique is the Significant Decimal Digit (SDD) [29–31, 38, 39], where the model order is estimated by:

$$\widehat{M}_{\text{SD}} = \arg \min_{i=1, \dots, L} \{ \sigma_i : \sigma_i / \sigma_{\max} \geq 10^{-p} \}, \quad (8)$$

where p is defined as the number of significant decimal digits in the data, σ_{\max} is the maximal singular value, and the singular values are assumed to be in descending order. Another closely related technique is the “gap” technique [33, 40], where the model order is estimated by:

$$\widehat{M}_{\text{GAP}} = \arg \max_{i=1, \dots, L-1} \{ \sigma_i / \sigma_{i+1} \}. \quad (9)$$

Although less mentioned in the MP literature, the information-theoretic based estimators (ITE) [3, 41, 42] can also be used:

$$\widehat{M}_{\text{ITE}} = \arg \min_{k=1, \dots, M_{\max}} \{ -\log(p_k(\mathbf{y}|\hat{\mathbf{v}}_k)) + kC(k, N) \}, \quad (10)$$

where M_{\max} is the maximum number of hypothesized exponentials (naturally, $M_{\max} \leq L$), $\mathbf{y} = \{y(n)\}_{n=0}^{N-1}$ is the vector of observations (1), and $p_k(\mathbf{y}|\hat{\mathbf{v}}_k)$ is the probability density function (PDF) of \mathbf{y} under the estimated parameter vector $\hat{\mathbf{v}}_k$, assuming the model order is k . Here, the estimated parameter vector is $\hat{\mathbf{v}}_k = [\{\hat{b}_i\}_{i=1}^k, \{\hat{\alpha}_i\}_{i=1}^k, \{\hat{\theta}_i\}_{i=1}^k]$, obtained by the MP method. The term $C(k, N)$ is a model-complexity penalty term, used as a regularization for maximum-likelihood based methods.

Remark 1. This is a coupled detection-estimation approach, which requires prior knowledge of the likelihood function.

B. Parameter estimation

Once we determine the model order \widehat{M} , we truncate the SVD of \mathbf{Y}_0 in (4) to rank \widehat{M} and use the eigenvalues of the resulting $\widehat{M} \times \widehat{M}$ matrix \mathbf{A} in (7) to estimate the signal poles. The estimated damping factor and normalized frequency are given by:

$$\hat{\alpha}_i = \log|\tilde{\lambda}_i|, \quad \hat{\theta}_i = \arg(\tilde{\lambda}_i), \quad i = 1, 2, \dots, \widehat{M} \quad (11)$$

Next, the amplitudes $\{b_i\}_{i=1}^{\widehat{M}}$ are estimated by solving the linear least squares problem [31]:

$$\hat{b}_i = \arg \min_{b_i} \sum_{n=0}^{N-1} |y(n) - \tilde{\lambda}_i^n b_i|^2, \quad (12)$$

which has a closed-form solution of:

$$\hat{\mathbf{b}} = \begin{bmatrix} 1 & 1 & \dots & 1 \\ \tilde{\lambda}_1 & \tilde{\lambda}_2 & \dots & \tilde{\lambda}_{\widehat{M}} \\ \tilde{\lambda}_1^2 & \tilde{\lambda}_2^2 & \dots & \tilde{\lambda}_{\widehat{M}}^2 \\ \vdots & \vdots & \ddots & \vdots \\ \tilde{\lambda}_1^{N-1} & \tilde{\lambda}_2^{N-1} & \dots & \tilde{\lambda}_{\widehat{M}}^{N-1} \end{bmatrix}^{\dagger} \begin{bmatrix} y(0) \\ y(1) \\ y(2) \\ \vdots \\ y(N-1) \end{bmatrix}, \quad (13)$$

where $(\cdot)^{\dagger}$ denotes the pseudo-inverse and $\hat{\mathbf{b}} = [\hat{b}_1, \hat{b}_2, \dots, \hat{b}_{\widehat{M}}]^T \in \mathbb{C}^{\widehat{M}}$.

C. The degenerate noiseless case

In the noiseless case, Hua et al. presented a complete theorem [29, Theorem 2.1], showing that the signal can be fully characterized using the noiseless MP solutions. Specifically, if $M \leq L \leq N - M$, the solutions $(\lambda, \mathbf{q}, \mathbf{p}^H)$ to the generalized noiseless eigenvalue problem:

$$(\mathbf{X}_1 - \lambda \mathbf{X}_0) \mathbf{q} = 0, \quad \mathbf{p}^H (\mathbf{X}_1 - \lambda \mathbf{X}_0) = 0, \quad (14)$$

such that $\mathbf{q} \in \text{Range}(\mathbf{X}_0^H)$ and $\mathbf{p} \in \text{Range}(\mathbf{X}_0)$ are $(z_i, \mathbf{q}_i, \mathbf{p}_i^H)$, where \mathbf{q}_i is the i -th column of

$$\mathbf{Z}_R^{\dagger} = \mathbf{Z}_R^H (\mathbf{Z}_R \mathbf{Z}_R^H)^{-1},$$

\mathbf{p}_i^H is the i -th row of

$$\mathbf{Z}_L^{\dagger} = (\mathbf{Z}_L^H \mathbf{Z}_L)^{-1} \mathbf{Z}_L^H,$$

and:

1) $\mathbf{Z}_L \in \mathbb{C}^{(N-L) \times M}$ is a Vandermonde matrix given by:

$$\begin{bmatrix} 1 & 1 & \dots & 1 \\ z_1 & z_2 & \dots & z_M \\ z_1^2 & z_2^2 & \dots & z_M^2 \\ \vdots & \vdots & \ddots & \vdots \\ z_1^{N-L-1} & z_2^{N-L-1} & \dots & z_M^{N-L-1} \end{bmatrix}. \quad (15)$$

2) $\mathbf{Z}_R \in \mathbb{C}^{M \times L}$ is a Vandermonde matrix given by:

$$\begin{bmatrix} 1 & z_1 & z_1^2 & \dots & z_1^{L-1} \\ 1 & z_2 & z_2^2 & \dots & z_2^{L-1} \\ \vdots & \vdots & \vdots & \ddots & \vdots \\ 1 & z_M & z_M^2 & \dots & z_M^{L-1} \end{bmatrix}. \quad (16)$$

The theorem is based on the following Vandermonde factorization of the noiseless Hankel matrices:

$$\begin{aligned} \mathbf{X}_0 &= \mathbf{Z}_L \mathbf{B} \mathbf{Z}_R, \\ \mathbf{X}_1 &= \mathbf{Z}_L \mathbf{B} \mathbf{Z}_R, \end{aligned} \quad (17)$$

where \mathbf{B} and \mathbf{Z} are $M \times M$ diagonal matrices comprising the signal's amplitudes and poles, respectively. For the proof and more details, see [29, Theorem 2.1].

As noted in [29], left-multiplying (14) by \mathbf{X}_0^{\dagger} , implies that the non-zero eigenvalues of the matrix $\mathbf{X}_0^{\dagger} \mathbf{X}_1 \in \mathbb{C}^{L \times L}$ are precisely the M signal poles, $\{z_i\}_{i=1}^M$. Furthermore, since the matrix $\mathbf{X}_0^{\dagger} \mathbf{X}_1 = \mathbf{Z}_R^{\dagger} \mathbf{Z} \mathbf{Z}_R$ has a rank of $M \leq L$, it also has $L - M$ zero eigenvalues with corresponding right eigenvectors in the null space of \mathbf{Z}_R .

While the MP theorem only addresses noiseless scenarios, practical situations involve noisy measurements. The impact of noise is substantial and current literature is built upon thresholding techniques of singular values, as discussed in II-A. However, in cases of closely-spaced frequencies and low SNR values in the threshold region, these techniques tend to underestimate or over-estimate the model order M (See Section VII). In Section III, we introduce the MP *modes*, which are derived by accounting for noise effects, and reveal the spectral

structure of the signal-related modes. This structure allows us to identify the signal-related modes and estimate M more accurately (see Section VI), eliminating the need for singular values thresholding employed in the decoupled approach.

III. INTRODUCING THE MP MODES

The traditional model order detection in the MP method relies on the SVD of $\mathbf{Y}_0 = \mathbf{U}\Sigma\mathbf{V}^H$, given in (4). However, we now demonstrate that \mathbf{Y}_0 can be further decomposed into a product of matrices, and the structure of these matrices can be leveraged to determine the model order. Recall that, in the noiseless case, the factorization in (17) consists of the matrices \mathbf{Z}_R and \mathbf{Z}_L , which are (i) Vandermonde matrices, and (ii) the pseudo-inverses of the right and left eigenvector matrices of the noiseless MP $\mathbf{X}_1 - \lambda\mathbf{X}_0$. To introduce a similar factorization in the noisy case, we first define the noisy counterparts of \mathbf{Z}_R and \mathbf{Z}_L using the SVD of \mathbf{Y}_0 from (4), as the MP modes:

Definition 1 (MP modes). Define the right MP modes as the rows of:

$$\tilde{\mathbf{Z}}_{R,un} := \mathbf{Q}^{-1}\mathbf{V}^H \in \mathbb{C}^{L \times L}. \quad (18)$$

Similarly, define the left MP modes as the columns of:

$$\tilde{\mathbf{Z}}_{L,un} := \mathbf{U}\Sigma\mathbf{Q} \in \mathbb{C}^{(N-L) \times L}, \quad (19)$$

where 'un' stands for 'un-normalized'.

We note that the notion of "modes" is new in the context of the MP method, but is borrowed from the related DMD approach [43, Chap. 1]. In the sequel, we demonstrate that these modes contain spectral information that can be utilized in the detection step. These matrices, are the pseudo-inverses of the right and left eigenvector matrices of the noisy MP $\mathbf{Y}_1 - \lambda\mathbf{Y}_0$, given according to (5) and (7) by:

$$\tilde{\mathbf{Z}}_{R,un}^\dagger = \mathbf{V}\mathbf{Q}, \quad (20)$$

$$\tilde{\mathbf{Z}}_{L,un}^\dagger = \mathbf{Q}^{-1}\Sigma^{-1}\mathbf{U}^H, \quad (21)$$

respectively. By normalizing $\tilde{\mathbf{Z}}_{R,un}$ and $\tilde{\mathbf{Z}}_{L,un}$ (See Appendix B in the Supplementary Materials (SM)) and combining them with the SVD of \mathbf{Y}_0 , we can express the data matrices \mathbf{Y}_0 and \mathbf{Y}_1 as follows:

$$\begin{aligned} \mathbf{Y}_0 &= \tilde{\mathbf{Z}}_L \tilde{\mathbf{B}} \tilde{\mathbf{Z}}_R, \\ \mathbf{Y}_1 &= \tilde{\mathbf{Z}}_L \tilde{\mathbf{B}} \tilde{\mathbf{\Lambda}} \tilde{\mathbf{Z}}_R, \end{aligned} \quad (22)$$

where $\tilde{\mathbf{Z}}_R$ and $\tilde{\mathbf{Z}}_L$ are the normalized modes, $\tilde{\mathbf{B}}, \tilde{\mathbf{\Lambda}} \in \mathbb{C}^{L \times L}$ are diagonal matrices containing the noisy amplitudes and poles, respectively. This decomposition forms a noisy analogous to the decomposition of \mathbf{X}_0 and \mathbf{X}_1 in (17). For more details see Appendix B in the SM, where we provide a comprehensive theorem that establishes the extension of the classical MP theorem to accommodate signals contaminated by noise. The next result shows that $\tilde{\mathbf{Z}}_L$ has a valuable structure (a similar argument applies to $\tilde{\mathbf{Z}}_R$, but is omitted for brevity).

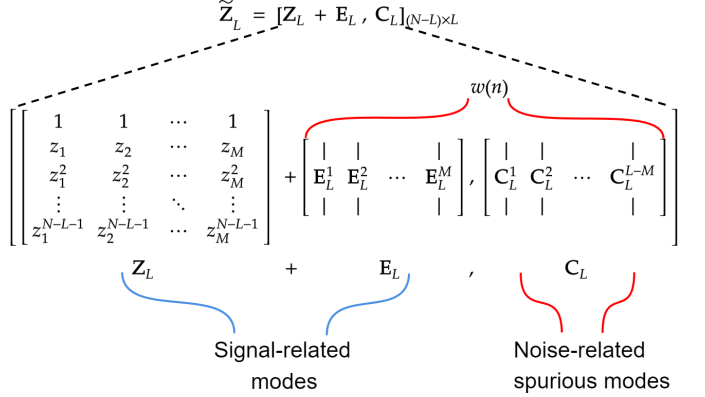


Fig. 1: The structure of $\tilde{\mathbf{Z}}_L$ by Proposition 1. The matrices \mathbf{E}_L and \mathbf{C}_L are a direct result of the additive noise $w(n)$.

Proposition 1. The matrix $\tilde{\mathbf{Z}}_L$, whose columns are the left MP modes, can be recast as

$$\tilde{\mathbf{Z}}_L = [\mathbf{Z}_L + \mathbf{E}_L, \mathbf{C}_L]_{(N-L) \times L}, \quad (23)$$

where the M leftmost columns of $\tilde{\mathbf{Z}}_L$ are the sum of the Vandermonde matrix $\mathbf{Z}_L \in \mathbb{C}^{(N-L) \times M}$ and a noise-related component, denoted by $\mathbf{E}_L \in \mathbb{C}^{(N-L) \times M}$. The remaining $L - M$ columns are noise-related spurious columns, denoted by $\mathbf{C}_L \in \mathbb{C}^{(N-L) \times (L-M)}$.

Proof. See Appendix B in the SM. \square

Signal and noise modes: in the noiseless case, the matrix \mathbf{Z}_L assumes a Vandermonde structure (15). In the noisy case, by (23), the matrix $\tilde{\mathbf{Z}}_L$ can be divided into two sub-matrices: the signal-related sub-matrix comprising the *signal modes*, represented by the M leftmost columns $\mathbf{Z}_L + \mathbf{E}_L$, and the noise-related sub-matrix comprising the *noise modes*, represented by the $L - M$ rightmost columns \mathbf{C}_L . In addition, each signal mode is a column of a Vandermonde matrix associated with a signal pole, obscured by the additive noise term \mathbf{E}_L . See Fig. 1 for illustration.

Critically, Proposition 1 is meaningful and has a practical value only when the noise term \mathbf{E}_L has a structure that allows accurate extraction of the Vandermonde structure. Therefore, in the sequel, we analyze the noise matrix \mathbf{E}_L . The analysis of \mathbf{E}_R follows similarly and is therefore omitted.

A. Analysis of the noise induced matrix \mathbf{E}_L

The analysis of \mathbf{E}_L is based on the analysis of the matrix $\mathbf{Y}_0^\dagger \mathbf{Y}_1$ as a perturbation of the matrix $\mathbf{X}_0^\dagger \mathbf{X}_1$, denoted by:

$$\mathbf{Y}_0^\dagger \mathbf{Y}_1 = \mathbf{X}_0^\dagger \mathbf{X}_1 + \delta(\mathbf{X}_0^\dagger \mathbf{X}_1). \quad (24)$$

Since the matrix $\mathbf{X}_0^\dagger \mathbf{X}_1$ has exactly M distinct non-zero eigenvalues and another $L - M$ zero eigenvalues, the Rank-Nullity Theorem guarantees that its eigenvectors form a basis. Let $\mathbf{T}_L^\dagger(\mathbf{X}_0^\dagger \mathbf{X}_1) \mathbf{T}_R = \mathbf{\Lambda}$ be the eigenvalue decomposition of $\mathbf{X}_0^\dagger \mathbf{X}_1$, where $\mathbf{\Lambda}$ is a diagonal matrix consisting of the eigenvalues $\{\lambda_k\}_{k=1}^L$, and \mathbf{T}_L and \mathbf{T}_R consist of the complete sets of left and right eigenvectors, $\{\mathbf{p}_k'\}_{k=1}^L$ and $\{\mathbf{q}_k'\}_{k=1}^L$, respectively, with $\mathbf{p}_k'^H \mathbf{q}_i' = 0$ for $k \neq i$. Without loss of

generality, suppose the eigenvalues $\{\lambda_i\}_{i=1}^M$ are the non-zero, simple, and equal the signal poles $\{z_i\}_{i=1}^M$, as guaranteed by the MP theorem for the noiseless case (Section II-C).

For a simple eigenvector \mathbf{q}_i' , let $\tilde{\mathbf{q}}_i'$ be its analogous perturbed eigenvector, which is an eigenvector of $\mathbf{Y}_0^\dagger \mathbf{Y}_1$ (see proof of Lemma 1 in Appendix A, for more details). Appropriate normalization of these eigenvectors is essential for the subsequent theoretical results, which is formulated in the following assumption.

Assumption 1. For $1 \leq i \leq M$, we assume that $\mathbf{p}_i^H \tilde{\mathbf{q}}_i' = 1$.

We remark that other alternative normalizations of $\tilde{\mathbf{q}}_i'$, such as $\tilde{\mathbf{q}}_i'^H \tilde{\mathbf{q}}_i' = 1$ or $\mathbf{q}_i'^H \tilde{\mathbf{q}}_i' = 1$, exists in the literature [44]. However, using such normalization will lead, in the sequel, to significant numerical errors due to the inversion of an ill-conditioned matrix. Next, we present a first-order approximation of the noise term \mathbf{E}_L with respect to the additive perturbation in (24), using \mathbf{W}_0 and \mathbf{W}_1 to represent the noise-related Hankel matrices formed by the additive noise $w(n)$.

Proposition 2. Under Assumption 1, the i -th column of $\mathbf{E}_L \in \mathbb{C}^{(N-L) \times M}$ defined in Proposition 1 is approximated by:

$$\mathbf{E}_L^i \cong \sum_{\substack{m=1 \\ m \neq i}}^M \frac{\mathbf{p}_m^H (\mathbf{W}_1 - z_i \mathbf{W}_0) \mathbf{q}_i}{b_i (\tilde{z}_i - z_m)} \begin{bmatrix} 1 \\ z_m \\ \vdots \\ z_m^{N-L-1} \end{bmatrix} + \frac{\mathbf{W}_0 \mathbf{q}_i}{b_i}, \quad (25)$$

provided that

$$\rho(\mathbf{D}_i \mathbf{T}_L^H \delta(\mathbf{X}_0^\dagger \mathbf{X}_1) \mathbf{T}_R) < 1, \quad (26)$$

where $\rho(\mathbf{A})$ is the spectral radius of the matrix \mathbf{A} , and the matrix \mathbf{D}_i is an $L \times L$ diagonal matrix defined by:

$$\mathbf{D}_i = \text{diag} \left(\frac{1}{\mathbf{p}_1^H \mathbf{q}_1' (\tilde{z}_i - \lambda_1)}, \dots, 0_i, \dots, \frac{1}{\mathbf{p}_L^H \mathbf{q}_L' (\tilde{z}_i - \lambda_L)} \right). \quad (27)$$

Proof. See Appendix C in the SM. \square

It is noteworthy that the condition in (26) and (27) implies a delicate balance between the i -th pole separation and perturbation (for details, see Remark 6 in Appendix C). In addition, note that the first term in the right hand side (r.h.s.) of (25) vanishes if $\mathbf{W}_1 = z_i \mathbf{W}_0$, i.e., when the noise signal $w(n)$ consists only of the signal pole z_i . In such a degenerate case, the noise coincides with one of the signal's poles. Finally, we remark that Proposition 2 does not imply that the noise term \mathbf{E}_L is small. However, in the sequel, we show that the structure of \mathbf{E}_L in (25) allows us to extract and exploit the obscured Vandermonde structure of the signal modes in $\tilde{\mathbf{Z}}_L^i$.

Using Propositions 1 and 2, any signal mode $\tilde{\mathbf{Z}}_L^i$, can be expressed as:

$$\tilde{\mathbf{Z}}_L^i = \mathbf{Z}_L^i + \mathbf{E}_L^i, \quad 1 \leq i \leq M, \quad (28)$$

where $\tilde{\mathbf{Z}}_L^i$, \mathbf{Z}_L^i and \mathbf{E}_L^i are the i -th columns of $\tilde{\mathbf{Z}}_L$, \mathbf{Z}_L and \mathbf{E}_L , respectively.

Let $\mathbf{Q}_i \in \mathbb{C}^{(N-L+1) \times N}$ be a convolution matrix, constructed from the vector $\mathbf{q}_i \in \mathbb{C}^{L \times 1}$, such that $\mathbf{Q}_i \mathbf{v} = \mathbf{q}_i * \mathbf{v}$ and $\mathbf{u}^T \mathbf{Q}_i = \mathbf{u}^T * \mathbf{q}_i$, for any two vectors $\mathbf{v} \in \mathbb{C}^{N \times 1}$

and $\mathbf{u} \in \mathbb{C}^{(N-L+1) \times 1}$. Additionally, denote by $\mathbf{a}(z)$ the Vandermonde column, of length $N-L$, build from z :

$$\mathbf{a}(z) = [1, z, \dots, z^{N-L-1}]^T. \quad (29)$$

Combining these notation with (28) and Proposition 2, we have the following result.

Corollary 1. Any signal mode $\tilde{\mathbf{Z}}_L^i$ can be recast as:

$$\tilde{\mathbf{Z}}_L^i \cong \mathbf{a}(z_i) + \sum_{\substack{m=1 \\ m \neq i}}^M \gamma_{i,m} \mathbf{a}(z_m) + \xi_i, \quad (30)$$

where

$$\gamma_{i,m} = \frac{\mathbf{u}_m^T \mathbf{Q}_i \mathbf{w}}{(\tilde{z}_i - z_m) b_i}, \quad \xi_i = \frac{\mathbf{I}_0 \mathbf{Q}_i \mathbf{w}}{b_i}, \quad (31)$$

the matrix \mathbf{I}_0 is given by:

$$\mathbf{I}_0 = [\mathbf{I}_{N-L}, \mathbf{0}]_{(N-L) \times (N-L+1)},$$

where \mathbf{I}_{N-L} is the identity matrix of size $N-L$ and $\mathbf{0} \in \mathbb{C}^{(N-L) \times 1}$ is the zero vector. The vector $\mathbf{u}_m \in \mathbb{C}^{(N-L+1)}$ is defined by:

$$\mathbf{u}_m^T = [0, \mathbf{p}_m^H] - z_i [\mathbf{p}_m^H, 0], \quad (32)$$

and $\mathbf{w} = [w(0), \dots, w(N-1)]^T$ is the discrete noise vector introduced in (1) with $\mathbb{E}[\mathbf{w} \mathbf{w}^H] = \sigma_w^2 \mathbf{I}_N$.

Equation (30) shows that the signal modes consist of the true mode \mathbf{Z}_L^i , corrupted by two factors: (i) superimposed $M-1$ modes \mathbf{Z}_L^m , $m \neq i$ weighted by the coefficients $\gamma_{i,m}$, and (ii) a noise term ξ_i . In the next result, we show that these two factors are controlled by the separation of the signal poles and the SNR at the i -th component, defined by:

$$\text{SNR}_i = \frac{|b_i|^2}{\sigma_w^2},$$

and in dB units as $\text{SNR}_{i,\text{dB}} = 10 \log_{10}(\text{SNR}_i)$.

Proposition 3. Under the conditions of Proposition 2, for any $\varepsilon \in (0, 1)$, the noise-related terms in (30) are bounded by:

$$|\gamma_{i,m}| \leq 2 \sqrt{\frac{2 \log(\frac{1}{\varepsilon})}{\text{SNR}_i}} \frac{\|\mathbf{u}_m * \mathbf{q}_i\|_2}{|z_i - z_m|}, \quad (33)$$

$$\|\xi_i\|_\infty \leq \sqrt{\frac{2 \log(\frac{1}{\varepsilon})}{\text{SNR}_i}}, \quad (34)$$

with a probability of at least $1 - \varepsilon$, provided that:

$$|z_i - z_m| \geq 2|\delta z_i|, \quad 1 \leq m \neq i \leq M. \quad (35)$$

Proof. See Appendix D in the SM. \square

Note that by (32), \mathbf{u}_m consists of the vector \mathbf{p}_m . Hence, the convolution $\|\mathbf{u}_m * \mathbf{q}_i\|_2$ in (33) implicitly depends on the poles and the distances between the poles, as the vectors \mathbf{p}_m^H and \mathbf{q}_i are given by the m -th row of \mathbf{Z}_L^\dagger and i -th column of \mathbf{Z}_R^\dagger , respectively. Additionally, we remark that the condition in (35) is common in perturbation analysis. Informally, this condition guarantees that the signal poles z_i are sufficiently distinct relative to their perturbations.

Proposition 3 implies that the coefficients of the corrupting factors in (30) can be bounded with high probability by a function of the SNR_i and the i -th pole separation, provided that the separation is sufficiently large. This allows us to present the following detection method, which is based on the structure of the signal modes in (30), and on $\|\mathbf{E}_L\|$.

IV. STRUCTURE-AWARE MODEL ORDER DETECTION

In this section, we propose a detection method by identifying the signal modes. By relying on the modes and the estimated poles for the detection, this approach fundamentally differs from existing approaches, where only the singular values are considered for the model order detection.

Based on Corollary 1, identifying the signal modes could be viewed as a relaxation of the original problem presented in (1) and (2); we are only interested in a *binary* classification, i.e., to determine whether the i -th mode is a signal mode or not, without parameter estimation. In turn, once the signal modes are identified, their corresponding eigenvalues enable us to estimate the signal parameters.

Specifically, we propose to detect the signal modes through a model-matching approach, by measuring the similarity of the modes to a pre-defined test vector.

A. Similarity Measure: Definition and Properties

According to (30) the i -th signal mode is modeled as a superposition of a Vandermonde vector built from the signal pole z_i , weighted Vandermonde vectors built from the other signal poles, and an additive noise terms. To exploit this model, we define a normalized similarity measure:

$$P_i(z) := \frac{|\mathbf{a}^H(z) \tilde{\mathbf{Z}}_L^i|^2}{\|\mathbf{a}(z)\|^2 \|\tilde{\mathbf{Z}}_L^i\|^2}, \quad 1 \leq i \leq L, \quad (36)$$

where $\mathbf{a}(z)$ is defined in (29), and analyze $P_i(z)$ for $1 \leq i \leq M$, where $\tilde{\mathbf{Z}}_L^i$ is a signal mode.

In the absence of noise, $\tilde{\mathbf{Z}}_L^i$ reduces to the Vandermonde vector \mathbf{Z}_L^i , and $P_i(z)$ attains a unique global maximum at the true signal pole, i.e., $P_i(z_i) = 1$. In the presence of noise, applying triangle and Cauchy–Schwarz inequalities to (36), we obtain the following bound on $P_i(z)$:

$$0 \leq \left(\frac{1 - \text{ISR}_i}{1 + \text{ISR}_i} \right)^2 \leq P_i(z_i) \leq 1, \quad (37)$$

where ISR_i is the Interference-to-Signal Ratio at the i -th mode:

$$\text{ISR}_i = \frac{\|\mathbf{E}_L^i\|}{\|\mathbf{a}(z_i)\|}. \quad (38)$$

The lower bound in (37) implies that, in the presence of noise, the similarity measure at the true signal pole, $P_i(z_i)$, attains high values when the ISR_i is small. Specifically, when $\text{ISR}_i \rightarrow 0$, $P_i(z_i) \rightarrow 1$.

By Prop. 3, the contributions of the other poles and the noise term in (30) are controlled by the problem parameters, making $\|\mathbf{E}_L^i\|$, and consequently, ISR_i , small under some conditions. Specifically, for any $\varepsilon \in (0, 1)$:

$$\text{ISR}_i \leq \sqrt{\frac{2 \log(\frac{2}{\varepsilon})}{\text{SNR}_i}} (2\Delta_i + 1) \frac{\sqrt{N - L}}{\|\mathbf{a}(z_i)\|}, \quad \text{w.p. } \geq 1 - \varepsilon, \quad (39)$$

where $\Delta_i = \sum_{m \neq i} \frac{\|\mathbf{u}_m * \mathbf{q}_i\|_2}{|z_i - z_m|}$. This inequality presents an explicit condition on the problem parameters for which ISR_i remains small, ensuring high values of $P_i(z_i)$.

Remark 2. If $z \in \mathbb{C}$ lies on the unit circle at the k -th Discrete Fourier Transform (DFT) frequency, $z = e^{\frac{j2\pi k}{N-L}}$, the test vector (29) becomes:

$$\mathbf{a}(z) = [1, e^{\frac{j2\pi k}{N-L}}, \dots, e^{\frac{j2\pi k(N-L-1)}{N-L}}]^T,$$

which coincides with the k -th column of a DFT matrix of length $N - L$. Therefore, in this case, the numerator of the similarity measure $P_i(z)$ in (36) is given by:

$$|\mathbf{a}^H(z) \tilde{\mathbf{Z}}_L^i|^2 = \left| \sum_{kn=0}^{N-L-1} \tilde{\mathbf{Z}}_L^i[n] e^{\frac{-j2\pi kn}{N-L}} \right|^2 = |\mathcal{F}(\tilde{\mathbf{Z}}_L^i)[k]|^2,$$

where $\mathcal{F}(\tilde{\mathbf{Z}}_L^i)[k]$ is the DFT of $\tilde{\mathbf{Z}}_L^i$ at the k -th frequency bin. This means that evaluating the numerator in (36) on the DFT grid is equivalent to analyzing the power spectrum of the mode, up to normalization.

B. The Detection Method

We propose to use the similarity measure $P_i(z)$ in (36) for identifying the signal modes. We showed above that the similarity measure at the true pole, $P_i(z_i)$, is high (under some conditions on the problem parameters), if the i -th mode $\tilde{\mathbf{Z}}_L^i$ is a signal mode. Since the true pole z_i is unknown, we compute the maximal value of $P_i(z)$:

$$\epsilon_i := P_i(z_i^*), \quad (40)$$

for $1 \leq i \leq L$, where

$$z_i^* = \underset{z \in \mathbb{C} \setminus \{0\}}{\operatorname{argmax}} P_i(z).$$

Intuitively, ϵ_i measures the maximal alignment between the i -th mode and the test vector $\mathbf{a}(z)$ defined in (29). Large values of ϵ_i indicate that $\tilde{\mathbf{Z}}_L^i$ is likely a structured signal mode, while small values suggest a spurious noise mode. More precisely, by (39), since $P_i(z_i^*) \geq P_i(z_i)$, signal modes yield large ϵ_i values, when a certain balance between the SNR_i , the i -th pole separation, the modes dimension $N - L$, and the i -th damping factor is maintained. This is illustrated in Fig. 2.

Remark 3. We emphasize that $P_i(z)$ is not used for estimating the poles, i.e., z_i^* is not considered an estimate of the pole, due to potential bias introduced by the noise terms in $\tilde{\mathbf{Z}}_L^i$. The poles are extracted from the eigenvalues associated with the identified signal modes.

The features $\{\epsilon_i\}_{i=1}^L$, computed in (40), are used to determine the order of the model by dividing them into two distinct subsets: signal-related and noise-related. The number of the signal-related modes then determines the model order. Since $\epsilon_i \geq P_i(z_i)$, the theoretical lower bound of $P_i(z_i)$ in (37) naturally serves as a mode-dependent threshold: the i -th mode is classified as signal mode if:

$$\left(\frac{1 - \text{ISR}_i}{1 + \text{ISR}_i} \right)^2 \leq \epsilon_i. \quad (41)$$

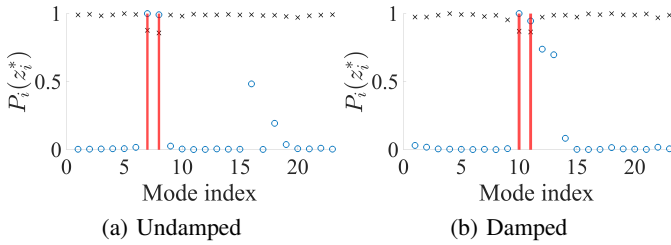


Fig. 2: Illustration of $P_i(z_i^*)$ for each mode $1 \leq i \leq L$, with a signal composed of two complex exponentials, $N = 71$, $b_1 = b_2 = 1$, and $|\theta_2 - \theta_1| = 2\pi/N$. In the damped case, $\alpha_1 = 0.03$ and $\alpha_2 = 0.05$. Red lines mark the signal modes; black crosses denote the lower bound (37). The SNR_{dB} = 10.

In summary, large values of ϵ_i , occur when ISR_i is small, indicate that $\tilde{\mathbf{Z}}_L^i$ is likely a structured signal mode. The lower bound in (37) yields a mode-dependent threshold, controlled by the problem parameters, for discerning between signal and noise modes, allowing model order detection by counting the signal modes.

C. Adjustment for Closely-spaced Poles

An additional advantage of determining the model order from the modes, rather than the singular values, is the ability to use additional information about the poles associated with each mode, which can be used to refine the features in (40).

When clusters of poles are present, neighboring modes can corrupt $P_i(z_i)$ due to high sidelobes of the Poisson kernel [45]. Specifically, the numerator of (36) is given by:

$$\mathbf{a}^H(z_i) \tilde{\mathbf{Z}}_L^i = \|\mathbf{a}(z_i)\|^2 + \sum_{\substack{m=1 \\ m \neq i}}^M \gamma_{i,m} \mathcal{P}(z_i, z_m) + \mathbf{a}^H(z_i) \boldsymbol{\xi}_i, \quad (42)$$

where $\mathcal{P}(z_i, z_m) = \sum_{n=0}^{N-L-1} (z_i^* z_m)^n$ denotes the finite-order Poisson kernel. This effect amplifies when z_i is close to other poles z_m and reduced when z_i is an isolated pole. To compensate for such leakage effects, we propose a normalized variant of (40):

$$\epsilon_i := \frac{1}{d_i} \cdot \max_{z \in \mathbb{C} \setminus \{0\}} P_i(z), \quad d_i = \sum_{m=1}^L |\tilde{\lambda}_m / \tilde{\lambda}_i|^2, \quad (43)$$

where $\tilde{\lambda}_m$ and $\tilde{\lambda}_i$ are the MP-estimated poles, d_i is interpreted as a measure of the poles concentration near $\tilde{\lambda}_i$, and ϵ_i is then normalized to the interval $[0, 1]$.

Remark 4. We leveraged the Vandermonde structure globally, by examining the similarity between the test vector in (29) and the modes. Alternatively, we could follow a local perspective, viewing each signal mode in (30) as a column of a perturbed Vandermonde matrix, demonstrating a near multiplicative structure. For example, in the context of DMD, Bronstein et al. [46] introduced a detection feature based on the mean ratio of consecutive rows of the DMD modes (see Appendix E in the SM for more details). Our simulations show that using the global features in (43) is superior to ‘local’ approaches, and therefore, their empirical results are not presented in the sequel.

V. EFFICIENT AMPLITUDES EXTRACTION

We propose a computationally efficient approach for estimating the amplitudes, leveraging the structure of the MP modes as described in Proposition 1 and more generally in Theorem 1, Appendix B. In these results, we show that the first row of the un-normalized left modes $\tilde{\mathbf{Z}}_{L,un}$ is given by:

$$\mathbf{e}_1^T \tilde{\mathbf{Z}}_{L,un} = \left[[\sqrt{b_1}, \dots, \sqrt{b_M}] + \mathbf{e}_1^T \mathbf{E}_L \sqrt{\mathbf{B}}, \mathbf{e}_1^T \mathbf{C}_L \right] \in \mathbb{C}^{1 \times L},$$

and similarly, the first column of the un-normalized right modes $\tilde{\mathbf{Z}}_{R,un}$ is given by:

$$\tilde{\mathbf{Z}}_{R,un} \mathbf{e}_1 = \left[[\sqrt{b_1}, \dots, \sqrt{b_M}]^T + \sqrt{\mathbf{B}} \mathbf{E}_R \mathbf{e}_1 \right] \in \mathbb{C}^{L \times 1}$$

where the vector \mathbf{e}_1 is the standard unit vector, and the matrices $\mathbf{C}_L \in \mathbb{C}^{(N-L) \times (L-M)}$, and $\mathbf{C}_R \in \mathbb{C}^{(L-M) \times L}$ are $L-M$ noise-related spurious columns and rows, respectively. Consequently, we propose to estimate the amplitudes by the following element-wise multiplication:

$$\hat{\mathbf{b}} = (\mathbf{e}_1^T \tilde{\mathbf{Z}}_{L,un})^T \odot (\tilde{\mathbf{Z}}_{R,un} \mathbf{e}_1) \in \mathbb{C}^L, \quad (44)$$

where $\hat{\mathbf{b}}$ consists of the estimated amplitudes, and the i -th entry of $\hat{\mathbf{b}}$ is given by:

$$\hat{b}_i = \begin{cases} b_i (1 + \mathbf{E}_L(1, i)) (1 + \mathbf{E}_R(i, 1)) & , \text{if } 1 \leq i \leq M, \\ \mathbf{C}_L(1, i-M) \mathbf{C}_R(i-M, 1) & , \text{if } M < i \leq L \end{cases}$$

This method involves simple element-wise multiplication of two vectors in \mathbb{C}^L , requiring $\mathcal{O}(L)$ operations. The existing method in (13) involves pseudo-inverting a matrix of size $N \times \widehat{M}$, where \widehat{M} is based on the truncated-SVD of \mathbf{Y}_0 , and hence $1 \leq \widehat{M} \leq L < N$. The computational complexity of the existing method is $\mathcal{O}(NM^2 + \widehat{M}^3)$. As noted in Section II, estimating the model order using the truncated-SVD step is prone to over- or underestimation. In the extreme case of underestimation, where $\widehat{M} = 1$, the existing method requires $\mathcal{O}(N)$ operations, while if $\widehat{M} = L$, the existing method requires $\mathcal{O}(NL^2 + L^3)$ operations. Either way, the proposed approach is more efficient. In Section VII, we compare its performances to the existing method for estimating the signal amplitudes given in (13), which is based on matrix inversion.

We highlight that similarly to Sec. IV, where spectral information is extracted from the MP modes to identify signal-related components, in (44), temporal information is extracted from the MP modes to estimate the noisy amplitudes efficiently. This new approach of extracting meaningful information from the MP modes fundamentally differs from existing approaches, where the MP modes (or eigenvectors) are not typically recognized as carrying valuable information for estimating the signal parameters.

VI. PROPOSED ALGORITHM

Relying on the analysis and results regarding model order detection and amplitude estimation in Sections IV and V, we present the Structure-Aware Matrix Pencil (SAMP) algorithm, which is summarized in Algorithm 1. Compared to the standard MP method, our main novelties are the detection of signal modes, a new model order detection approach, and efficient amplitude estimation.

A. Practical Considerations

(i) *Weak truncation.* Although the proposed model order detector does not require truncation in (4), it is known, and supported by our numerical studies, that removing strong noise-related components reduces the noise effects in the estimates [31, 47]. Therefore, we recommend applying a weak truncation in (4) to eliminate strong noise components only. Alternatively, one can assume, for example, that $2M \leq L$ and truncate the smallest $\lfloor \frac{L}{2} \rfloor$ singular values in (4). In our setup, we do not assume prior knowledge of M , and by our simulations, an example of a weak-truncation method is the effective rank method, introduced in [48].

The effective rank method estimates the dimensionality or rank of a matrix in the presence of noise by utilizing the entropy of its normalized singular values. Given a set of singular values $\{\sigma_i\}_{i=1}^L$, the normalized singular values are defined as $\bar{\sigma}_i = \frac{\sigma_i}{\sum_{j=1}^L \sigma_j}$. The entropy $H(\bar{\sigma})$ of these normalized singular values is calculated using $H(\bar{\sigma}) = -\sum_{i=1}^n \bar{\sigma}_i \log(\bar{\sigma}_i)$, and the effective rank is then defined as $\exp(H(\bar{\sigma}))$. The model order is estimated by:

$$\widehat{M}_{\text{ER}} = \text{round}(\exp(H(\bar{\sigma}))). \quad (45)$$

We highlight that the proposed SAMP algorithm remains valid without truncation, at the cost of increased bias at high SNR levels.

(ii) *Practical threshold for ϵ_i .* While the threshold in (41) provides a theoretically grounded criterion for identifying the signal modes, estimating ISR_i in practice is challenging. To address this, we propose a simplified variant of the detection rule in (41). Using the structure of \mathbf{E}_L^i in Proposition 2, we observe that $\|\mathbf{E}_L^i\|$ is inversely proportional to $|b_i|$, and therefore, the ISR_i can be written as:

$$\text{ISR}_i = \frac{c_i}{|b_i| \|\mathbf{a}(z_i)\|},$$

where $c_i \in \mathbb{R}$ is a tunable parameter, capturing the remaining terms in $\|\mathbf{E}_L^i\|$. Since the true amplitudes and poles b_i and z_i are unknown, we use their estimates \hat{b}_i and $\tilde{\lambda}_i$, and define the following simplified amplitude-based threshold: the i -th mode is classified as signal mode if:

$$\left(\frac{1 - c_i / |\hat{b}_i| \|\mathbf{a}(\tilde{\lambda}_i)\|}{1 + c_i / |\hat{b}_i| \|\mathbf{a}(\tilde{\lambda}_i)\|} \right)^2 \leq \epsilon_i, \quad (46)$$

where we set $c_i = 10\sqrt{N - L}$ in our experiments. Notably, c_i may also be tuned individually per mode to improve flexibility. This rule respects the structure of the theoretical rule in (41), while relying only on quantities available in practice.

Remark 5. *The proposed SAMP algorithm (Algorithm 1) deviates from the conventional “detect and then estimate” strategy. Instead, it adopts an “estimate and then select” approach, wherein the model parameters are first estimated from the eigenvalues and modes, and then, the signal-related components selected based on these estimated parameters.*

Algorithm 1 SAMP proposed algorithm

Input: Noisy measurements $\{y(n)\}_{n=0}^{N-1}$, pencil parameter L , and the tunable parameters $\{c_i\}_{i=0}^L$.

Output: Estimates of the signal frequencies, damping factors, and amplitudes.

1: Modes and Eigenvalues Computation:

- Construct the Hankel matrices $\mathbf{Y}_0, \mathbf{Y}_1$ from the measured signal $\{y(n)\}_{n=0}^{N-1}$ by (3).
- Compute the truncated-SVD of $\mathbf{Y}_0 \approx \mathbf{U}\Sigma\mathbf{V}^H$, using the effective-rank method by (45).
- Decompose the matrix $\mathbf{A} = \Sigma^{-1}\mathbf{U}^H\mathbf{Y}_1\mathbf{V}$ to get $\mathbf{A}\mathbf{Q} = \mathbf{Q}\tilde{\Lambda}$, by (7).
- Calculate the left MP modes $\tilde{\mathbf{Z}}_L = \mathbf{U}\Sigma\mathbf{Q}$ by (19).

2: Parameter Estimation:

- Estimate the frequencies and damping factors by (11):

$$\hat{\theta}_i = \arg(\tilde{\lambda}_i), \quad \hat{\alpha}_i = \log|\tilde{\lambda}_i|, \quad 1 \leq i \leq L.$$

- Estimate the complex amplitudes by (44):

$$\hat{\mathbf{b}} = (\mathbf{e}_1^T \tilde{\mathbf{Z}}_L)^T \odot (\tilde{\mathbf{Z}}_L \mathbf{e}_1)$$

3: Model Order Detection:

- Compute the L features by (43):

$$\epsilon_i = \frac{1}{d_i} \cdot \max_{z \in \mathbb{C} \setminus \{0\}} P_i(z), \quad 1 \leq i \leq L,$$

and normalize them to the interval $[0, 1]$.

- Partition the features into two distinct subsets by defining the signal-related subset as the subset of features satisfying (46):

$$\left(\frac{1 - c_i / |\hat{b}_i| \|\mathbf{a}(\tilde{\lambda}_i)\|}{1 + c_i / |\hat{b}_i| \|\mathbf{a}(\tilde{\lambda}_i)\|} \right)^2 \leq \epsilon_i.$$

- Set the model order to: $\widehat{M} = |\mathcal{S}|$, where \mathcal{S} is the set of indices corresponding to the signal-related subset.

4: Parameter Selection:

- Select the signal components by: $\hat{\theta}_s, \hat{\alpha}_s, \hat{b}_s, \quad s \in \mathcal{S}$.
-

B. Computational complexity

We evaluate the computational complexity of the proposed algorithm by counting the number of complex operations required for each step. In step 1, we compute the modes and eigenvalues. This step requires $\mathcal{O}((N - L)L^3)$ operations. In step 2, we estimate the signal parameters. This step requires $\mathcal{O}(L)$ operations. In step 3, we determine the model order. First we compute the L measures $\{\epsilon_i\}_{i=1}^L$ using (43), which requires $\mathcal{O}((N - L)^2)$ operations. Next, we divide the set $\{\epsilon_i\}_{i=1}^L$ into two distinct subsets, which requires $\mathcal{O}(L)$ operations. In step 4, we select the signal-related parameters. This step requires $\mathcal{O}(\widehat{M})$ operations. The overall complexity of the proposed algorithm is $\mathcal{O}((N - L)^2 + (N - L)L^3)$. For comparison, the overall complexity of the standard MP algorithm is also $\mathcal{O}((N - L)L^3)$, and the most demanding step in both methods is the calculation of the matrix \mathbf{A} which involves the multiplication of four matrices.

VII. NUMERICAL RESULTS

In this section, we present simulation results focusing on closely-spaced frequencies under various SNR levels. We begin by showcasing the detection and estimation capabilities of the proposed SAMP algorithm (Algorithm 1). Then, we demonstrate the proposed amplitude estimation method and compare it in terms of computation time and accuracy to the traditional amplitude estimation method in (13).

We compare the proposed SAMP algorithm with five other methods based on singular value truncation. Two methods are based on ITE: AIC [3] and EVT [42] criteria. These methods use the *coupled detection and estimation* approach, which requires prior knowledge of the noise distribution (that is unknown in our setting), and involves computing the likelihood function for every possible hypothesized model order, making them computationally inefficient, as will be evident in the sequel. The EVT criterion is used because it was shown to outperform the common MDL and MAP criteria, and to be less sensitive to noise model mismatch [42].

The remaining baseline methods use the *decoupled detection and estimation* approach, which is the standard practice in the MP literature. In particular, we examine the Significant Decimal Digits (SDD) method (see Section II-A), a widely used method in the MP literature [29–31, 38, 39]. Additionally, we evaluate the GAP method, introduced in Sec. II-A, which is another common approach for SVD truncation [33, 40]. For a fair comparison, we also include the effective rank method (EFF) [48], as we use it in our algorithm as a pre-processing step to eliminate strong noise-related components.

Throughout this section, we simulate two scenarios involving two and four closely-spaced complex exponentials, generated according to (2). In both cases, $\{b_i = 1\}_{i=1}^M$, and $L = \text{round}(N/3)$. In each scenario, we conduct two experiments. The first involves *undamped* exponentials, with $\{\alpha_i = 0\}_{i=1}^M$. The second involves *damped* exponentials: for the two-components case, we set $\alpha_1 = 0.03$, and $\alpha_2 = 0.05$; for the four-components case, we set $\alpha_1 = \alpha_3 = 0.03$, and $\alpha_2 = \alpha_4 = 0.05$. Our goal is twofold. Given a finite sample of the noisy signal $y(n)$, as in (1), we aim to detect the model order (the number of complex exponentials), which is $M = 2$ or $M = 4$ in our simulations, and estimate the corresponding M frequencies, damping factors, and amplitudes. The code to reproduce all the results in this section is available in the following GitHub link.

A. Model order detection

We determine the probability of correctly identifying the model order, p_d , defined by:

$$p_d = \mathbb{P}(\widehat{M} = M) \cong \frac{1}{N_{\text{exp}}} \sum_{i=1}^{N_{\text{exp}}} \mathbb{1}_{\widehat{M}=M},$$

where $N_{\text{exp}} = 500$ is the number of independent Monte-Carlo trials, and $\mathbb{1}_{\widehat{M}=M}$ is an indicator function that equals 1 if the estimated model order \widehat{M} matches the true model order M , and 0 otherwise. To simplify comparisons, we report the Area Under the Curve (AUC) for each method.

Fig. 3 displays the probability of correct detection p_d as a function of the SNR in dB for $N = 71$ samples. In Figs. 3a-3b, we simulate $M = 2$ exponentials, with $\theta_1 = 2$ rad/sample, and $\theta_2 = \theta_1 + \frac{2\pi}{N}$. In Figs 3c-3d, we simulate $M = 4$ exponentials, divided into two clusters, with $\theta_1 = 2$ rad/sample, $\theta_2 = \theta_1 + \frac{2\pi}{N}$, and $\theta_3 = -\theta_1$, $\theta_4 = -\theta_2$. The value of θ_2 is set because the difference $|\theta_2 - \theta_1| = \frac{2\pi}{N}$ is the Rayleigh limit [49]. We note that theoretical frequency resolution limits are also discussed in [50, 51]. The SNR is defined as:

$$\text{SNR} = \sum_{i=1}^M \frac{|b_i|^2}{\sigma_w^2},$$

and we denote $\text{SNR}_{\text{dB}} = 10\log_{10}(\text{SNR})$. Fig. 4 displays p_d versus the number of samples N for SNR_{dB} of 8 dB. We simulate $M = 2$ exponentials in Figs. 4a-4b and $M = 4$ exponentials in 4c-4d, where the frequencies spacing is the same as in Fig. 3. Fig. 5 displays p_d versus the frequencies spacing $|\Delta\theta|$ for SNR_{dB} value of 10 dB and $N = 71$ samples. We simulate $M = 2$ exponentials in Figs. 5a-5b and $M = 4$ exponentials in 5c-5b, divided into two clusters. In the case of $M = 4$, the varying frequencies spacing is within each cluster: $|\Delta\theta| = |\theta_2 - \theta_1| = |\theta_4 - \theta_3|$.

The proposed SAMP method outperforms the GAP, SDD, and EFF methods by a wide margin in all the presented scenarios. We note that the EFF method fails as a stand-alone detection method, but we use it as a pre-processing step in the proposed SAMP method to eliminate strong noise components. Empirically, we see that the EFF method consistently overestimates the model order, even at high SNR_{dB} values. Additionally, the SAMP method also outperforms the EVT and AIC criteria in all the presented cases. When comparing the undamped and damped cases, we observe a general degradation in performance; however, the relative trends remain the same, with SAMP outperforming all the baseline methods.

Noise distribution effects: To assess the impact of deviations from the Gaussian noise assumption, we also simulate non-Gaussian additive noise. Table I shows the AUC of p_d versus the SNR_{dB} (in the range of $[-10, 20]$ dB), for each method under both normal and bi-normal noise distributions, in the case of $M = 2$ (the complementary results for $M = 4$ show similar trends and are omitted for brevity). The first experiment (second column from left) depicts the results of a normal distribution, as seen in Figs. 3a-3b. In the second experiment (third column from left), we simulated a Bi-normal distribution:

$$\mathcal{B}_d = \mathbb{1}_{p < r} \cdot \mathcal{N}(\mu_1, \sigma_1) + \mathbb{1}_{p \geq r} \cdot \mathcal{N}(\mu_2, \sigma_2),$$

where p is a random number drawn from the standard uniform distribution on the open interval $(0, 1)$, and r is a pre-defined threshold, set to $r = 0.85$ in our simulations. The results demonstrate that SAMP is moderately sensitive to deviations from the assumed noise distribution, with an average degradation of approximately 5%. In contrast, ITE methods such as EVT and AIC are more affected, with an averaged degradation of approximately 14% to EVT and 17% to AIC. Interestingly, GAP remains largely insensitive, likely due to its reliance solely on spectral thresholding, but its detection capabilities

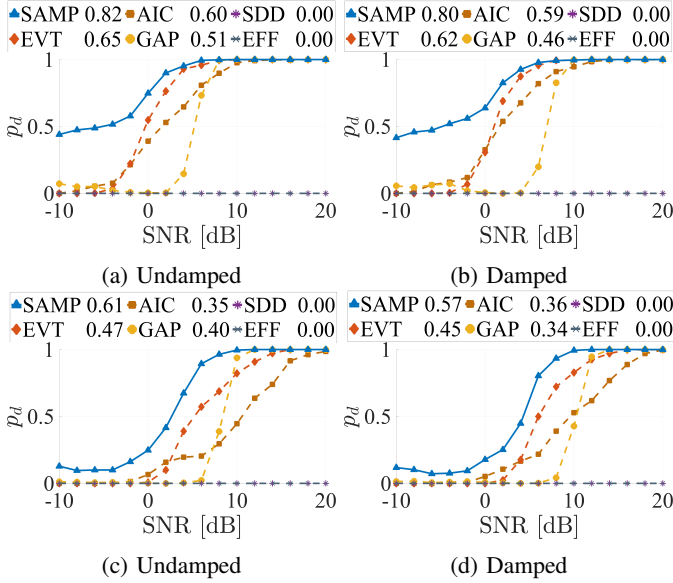


Fig. 3: Probability of correct model order estimation versus SNR_{dB} , for $M = 2$ in (a)-(b), and $M = 4$ in (c)-(d). AUC scores are provided in the legend.

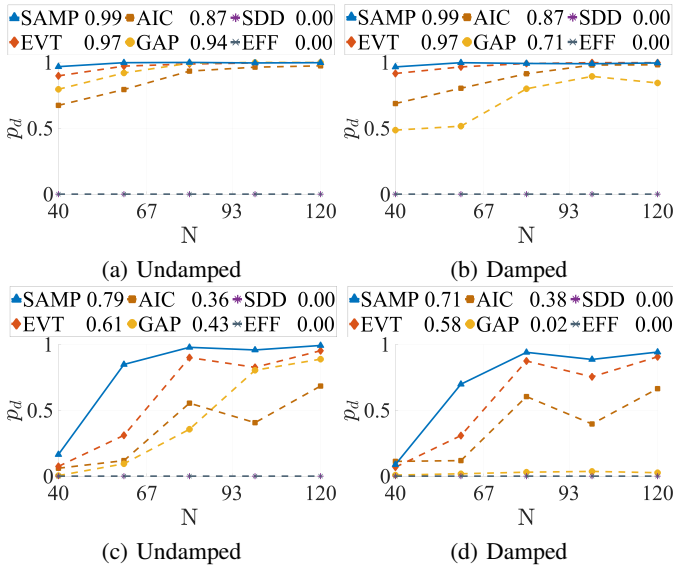


Fig. 4: Probability of correct model order estimation versus the number of samples N , for $M = 2$ in (a)-(b), and $M = 4$ in (c)-(d). The SNR_{dB} is 8 dB, and the AUC scores are provided in the legend.

are low. Due to poor performance, the SDD and EFF methods yield AUC values near zero and cannot be analyzed.

B. Parameter estimation

We evaluate the empirical bias and the Root Mean Squared Error (RMSE) of an estimate $\hat{\eta}$ of a parameter of interest η which are defined by:

$$\text{bias}(\hat{\eta}) = \frac{1}{N_{\text{exp}}} \sum_{i=1}^{N_{\text{exp}}} \hat{\eta}_i - \eta, \quad \text{RMSE}(\hat{\eta}) = \sqrt{\frac{1}{N_{\text{exp}}} \sum_{i=1}^{N_{\text{exp}}} (\hat{\eta}_i - \eta)^2}$$

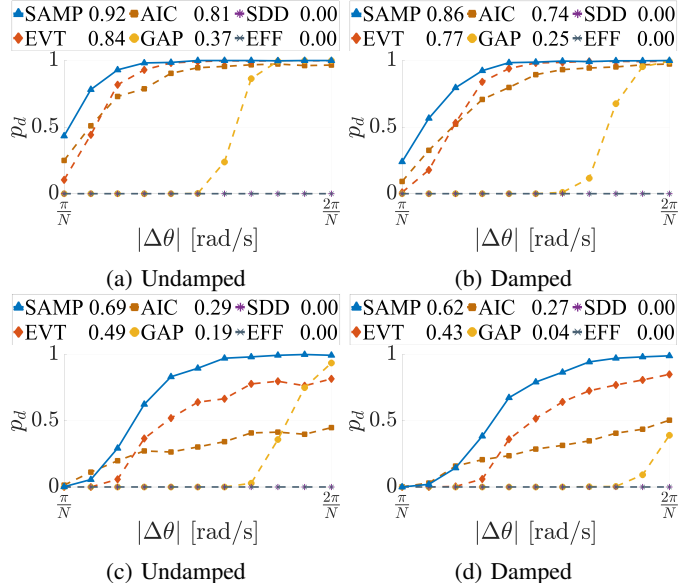


Fig. 5: Probability of correct model order estimation versus the frequency separation, for $M = 2$ in (a)-(b), and $M = 4$ in (c)-(d). AUC scores are provided in the legend.

TABLE I: AUC comparison of the different methods under normal and bi-normal noise distributions, for the undamped (undmp) and damped (dmp) cases.

Method	Normal		Bi-normal	
	undmp	dmp	undmp	dmp
SAMP	0.82	0.80	0.78	0.76
EVT	0.65	0.62	0.56	0.53
AIC	0.60	0.59	0.50	0.49
GAP	0.51	0.46	0.52	0.46
SDD	0.00	0.00	0.00	0.00
EFF	0.00	0.00	0.00	0.00

where $\{\hat{\eta}_i\}_{i=1}^{N_{\text{exp}}}$ is the estimate of η in the i -th Monte-Carlo trial, and $N_{\text{exp}} = 500$ is the number of independent Monte-Carlo trials. In cases of model order mismatch in the detection step, we assign a fixed penalty to the corresponding trial. This penalty is proportional to the range of η , and scaled according to the X-axis of the current evaluation. For example, if the RMSE is evaluated versus the number of samples N , the penalty is normalized by N . This ensures fair penalization across different ranges of the evaluation variable.

Fig. 6 displays the average RMSE in dB of the estimates $\{\hat{\theta}_i\}_{i=1}^M$ versus the SNR_{dB} . The complementary figures of the average empirical bias are presented in Fig. 9 in Appendix F. We include the Cramer-Rao lower bound (CRB) as a reference for evaluating the average variance of $\{\hat{\theta}_i\}_{i=1}^M$ (see [3, 4] for details). All the competing methods show nearly unbiased estimates for SNR_{dB} values above a certain threshold, as shown in Fig. 9 in Appendix F. Therefore, following the approach presented in [33], we use the CRB for an unbiased estimator as a reference for the competing methods. For unbiased estimators, the RMSE simplifies to the square root

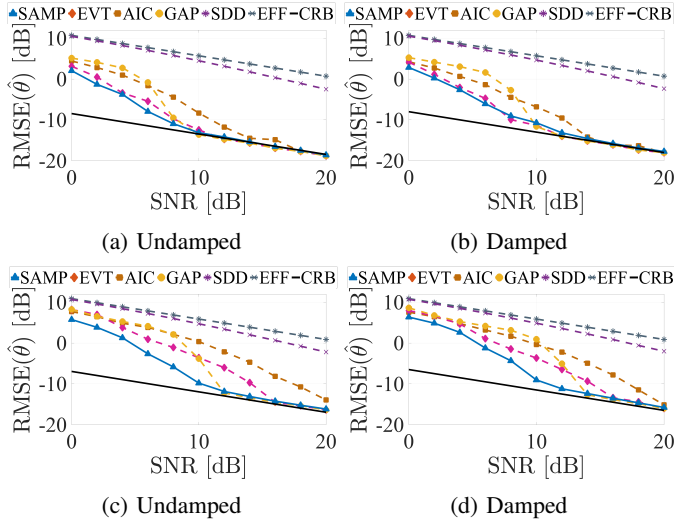


Fig. 6: Average RMSE of $\{\hat{\theta}_i\}_{i=1}^M$ versus the SNR_{dB}, for $M = 2$ in (a)-(b), and $M = 4$ in (c)-(d).

of the variance, since $\text{RMSE}^2(\hat{\theta}_1) = \text{var}(\hat{\theta}_1) + \text{bias}^2(\hat{\theta}_1)$.

Figures 6a-6d, shows that the SAMP method achieves the lowest or comparable RMSE for SNR below a threshold. For $M = 2$, SAMP and EVT are the two best performers, with SAMP showing slightly better results for SNR below 6 dB. For $M = 4$, the separation between methods is larger: SAMP consistently yields the lowest RMSE up to 12 dB, whereas EVT, AIC and GAP exhibit noticeably higher errors, especially at moderate SNR values. The SDD, and EFF exhibit significantly higher RMSE across all regimes. Overall, damping in Fig. 6b and 6d, degrades performance but does not change the ranking; SAMP is the the most accurate for $M = 4$ and is comparable to EVT for $M = 2$.

The complementary results of the average RMSE in dB and the absolute value of the average empirical bias of the estimates $\{\hat{\theta}_i\}_{i=1}^M$ versus the number of samples N , and the frequencies separation show similar trends and are presented in Fig. 10 and Fig. 11, respectively, in Appendix F.

C. Computational Load

To compare the computational cost of the proposed SAMP Algorithm with the baseline methods, we present the computation time as a function of the signal length in Fig. 7. The results show that the SAMP method achieves lower computational time than the EVT and AIC methods, but higher than the GAP and SDD methods. This behavior is expected: ITE methods require evaluating the likelihood function for all candidate model orders $1 \leq \widehat{M} \leq L$, while spectral thresholding typically involve only $\mathcal{O}(L)$ operations, which is fewer than those required by SAMP, as detailed in Section VI-B.

D. Amplitudes Estimation

In (44) in Section VI, we presented a computationally efficient approach for estimating the noisy amplitudes. We evaluate the performance of our method in comparison to the standard amplitude estimation technique presented in (13). We

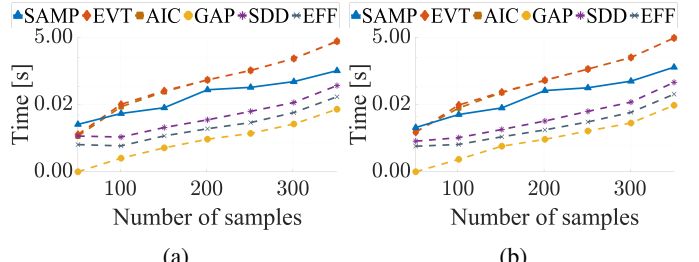


Fig. 7: Computational time (in log scale) versus number of samples for SAMP and baseline methods. $M = 2$ in (a), and $M = 4$ in (b). The SNR_{dB} is 10 dB.

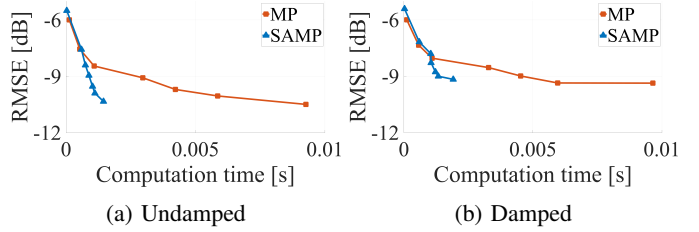


Fig. 8: Computational time comparison between the proposed amplitude estimation method, and the standard amplitude estimation method. The frequencies spacing is the Rayleigh limit, and the SNR_{dB} is 10 dB.

set $r = L$ to concentrate only on the amplitude estimation, circumventing any possible overestimation or underestimation of the model order by any of the methods.

Fig. 8 displays the amplitude estimation error for each method as a function of the computation time for different signal lengths in the case of $M = 4$. The error is defined as the sum of the RMSE between each of the true amplitudes and the closest two estimated amplitudes. We see in the figure that the proposed method obtains the same RMSE level as the standard method (except for the first simulated point) in considerably lower computation time. The complementary case of $M = 2$ shows similar trends and is omitted for brevity.

Conclusion We addressed the problem of detecting the number of complex exponentials and estimating their parameters from noisy measurements using the MP method. We introduced the concept of MP *modes*, through an extension of the MP theorem to noisy conditions, revealing their informative structure. Specifically, we showed that the signal-related modes can be expressed as an obscured Vandermonde matrix, $\mathbf{Z}_L + \mathbf{E}_L$, and provided a detailed characterization of the noise term \mathbf{E}_L .

By leveraging the spectral structure of the signal-related modes and utilizing the noise-term characterization, we showed that temporal information can be effectively extracted, significantly improving model order selection, which often solely relies on singular values and thresholding. Utilizing the MP modes, we proposed the SAMP algorithm for detecting and estimating the signal-related components, and a computationally efficient method for estimating the signal's amplitudes. A key advantage of using the MP modes lies in its ability to capture the temporal information encoded in the relationship

between \mathbf{Y}_0 and \mathbf{Y}_1 . In contrast, singular values are computed solely from \mathbf{Y}_0 and therefore miss this temporal information.

Our simulations indicate that the proposed method outperforms the classical thresholding-based competing methods by a large margin in detecting the model order, and nearly achieves the CRB for a SNR above a threshold, in estimating the signal's parameters. When compared to *coupled detection-estimation* approaches, such as EVT and AIC, the proposed method achieves comparable or better results with significantly lower computational time. Additionally, unlike EVT and AIC, the proposed method does not require prior knowledge of the noise distribution and was shown to be much less sensitive to noise model mismatch.

We postulate that our approach is general, and it is not restricted to the MP method only. For example, several related methods generate Hankel matrices similar to the MP method and use a truncated SVD step to reduce noise. These include the SVD-based Prony method [52], State Space method (SSM) [53], Dynamic Mode Decomposition (DMD) [34], and Singular Spectrum Analysis (SSA) [54, 55].

In future research, we will extend these findings to multivariate signals and explore the concept of *modes* in other super-resolution methods, such as ESPRIT [9].

REFERENCES

- [1] D. B. Percival and A. T. Walden, *Spectral analysis for physical applications*. cambridge university press, 1993.
- [2] S. M. Kay and S. L. Marple, "Spectrum analysis—a modern perspective," *Proc. IEEE*, vol. 69, no. 11, pp. 1380–1419, 1981.
- [3] P. Stoica, R. L. Moses, et al., *Spectral analysis of signals*. Pearson Prentice Hall Upper Saddle River, NJ, 2005, vol. 452.
- [4] S. Lang and J. McClellan, "Frequency estimation with maximum entropy spectral estimators," *IEEE Trans. Acoust. Speech Signal Process.*, vol. 28, no. 6, pp. 716–724, 1980.
- [5] T. Abatzoglou, "A fast maximum likelihood algorithm for frequency estimation of a sinusoid based on newton's method," *IEEE Trans. Acoust. Speech Signal Process.*, vol. 33, no. 1, pp. 77–89, 1985.
- [6] Y. Bresler and A. Macovski, "Exact maximum likelihood parameter estimation of superimposed exponential signals in noise," *IEEE Trans. Acoust. Speech Signal Process.*, vol. 34, no. 5, pp. 1081–1089, 1986.
- [7] J. Capon, "High-resolution frequency-wavenumber spectrum analysis," *Proc. IEEE*, vol. 57, no. 8, pp. 1408–1418, 1969.
- [8] R. Schmidt, "Multiple emitter location and signal parameter estimation," *IEEE Trans. Antennas Propag.*, vol. 34, no. 3, pp. 276–280, 1986.
- [9] R. Roy and T. Kailath, "Esprit-estimation of signal parameters via rotational invariance techniques," *IEEE Trans. Acoust. Speech Signal Process.*, vol. 37, no. 7, pp. 984–995, 1989.
- [10] P. Stoica and K. C. Sharman, "Maximum likelihood methods for direction-of-arrival estimation," *IEEE Trans. Acoust. Speech Signal Process.*, vol. 38, no. 7, pp. 1132–1143, 1990.
- [11] P. Stoica, P. Babu, and J. Li, "New method of sparse parameter estimation in separable models and its use for spectral analysis of irregularly sampled data," *IEEE Trans. Signal Process.*, vol. 59, no. 1, pp. 35–47, 2010.
- [12] L. Hu, Z. Shi, J. Zhou, and Q. Fu, "Compressed sensing of complex sinusoids: An approach based on dictionary refinement," *IEEE Trans. Signal Process.*, vol. 60, no. 7, pp. 3809–3822, 2012.
- [13] M. F. Duarte and R. G. Baraniuk, "Spectral compressive sensing," *Appl. Comput. Harmon. Anal.*, vol. 35, no. 1, pp. 111–129, 2013.
- [14] G. Tang, B. N. Bhaskar, P. Shah, and B. Recht, "Compressed sensing off the grid," *IEEE Trans. Inf. Theory*, vol. 59, no. 11, pp. 7465–7490, 2013.
- [15] L. Hu, J. Zhou, Z. Shi, and Q. Fu, "A fast and accurate reconstruction algorithm for compressed sensing of complex sinusoids," *IEEE Trans. Signal Process.*, vol. 61, no. 22, pp. 5744–5754, 2013.
- [16] Z. Yang, J. Li, P. Stoica, and L. Xie, "Sparse methods for direction-of-arrival estimation," in *Academic Press Library in Signal Process., Volume 7*, Elsevier, 2018, pp. 509–581.
- [17] Y. Chu, Z. Wei, and Z. Yang, "New reweighted atomic norm minimization approach for line spectral estimation," *Signal Process.*, vol. 206, p. 108897, 2023.
- [18] X. Wu, Z. Yang, J.-F. Cai, and Z. Xu, "Spectral super-resolution on the unit circle via gradient descent," in *Int. Conf. on Acoust. Speech Signal Process. (ICASSP)*, IEEE, 2023, pp. 1–5.
- [19] F. Andersson, M. Carlsson, J.-Y. Tourneret, and H. Wendt, "Frequency estimation based on hankel matrices and the alternating direction method of multipliers," in *21st European Signal Process. Conf. (EUSIPCO 2013)*, IEEE, 2013, pp. 1–5.
- [20] B. Hayes, C. Saitis, and G. Fazekas, "Sinusoidal frequency estimation by gradient descent," in *Int. Conf. on Acoust. Speech Signal Process. (ICASSP)*, IEEE, 2023, pp. 1–5.
- [21] P. Verma and R. W. Schafer, "Frequency estimation from waveforms using multi-layered neural networks," in *INTERSPEECH*, 2016, pp. 2165–2169.
- [22] G. Izacard, S. Mohan, and C. Fernandez-Granda, "Data-driven estimation of sinusoid frequencies," *Advances in Neural Information Process. Syst.*, vol. 32, 2019.
- [23] G. Izacard, B. Bernstein, and C. Fernandez-Granda, "A learning-based framework for line-spectra super-resolution," in *Int. Conf. on Acoust. Speech Signal Process. (ICASSP)*, IEEE, 2019, pp. 3632–3636.
- [24] Y. Xie, M. B. Wakin, and G. Tang, "Data-driven parameter estimation of contaminated damped exponentials," in *2021 55th Asilomar Conf. on Signals, Syst., and Computers*, IEEE, 2021, pp. 800–804.
- [25] P. Pan, Y. Zhang, Z. Deng, and W. Qi, "Deep learning-based 2-d frequency estimation of multiple sinusoids,"

- [25] *IEEE Trans. Neural Networks Learn. Syst.*, vol. 33, no. 10, pp. 5429–5440, 2021.
- [26] P. Pan, Y. Zhang, Z. Deng, and G. Wu, “Complex-valued frequency estimation network and its applications to superresolution of radar range profiles,” *IEEE Trans. Geosci. Remote Sens.*, vol. 60, pp. 1–12, 2021.
- [27] J. W. Smith and M. Torlak, “Frequency estimation using complex-valued shifted window transformer,” *IEEE Geosci. Remote Sens. Lett.*, 2024.
- [28] B. Porat, *A course in digital signal processing*. John Wiley & Sons, Inc., 1996.
- [29] Y. Hua and T. K. Sarkar, “Matrix pencil method for estimating parameters of exponentially damped/undamped sinusoids in noise,” *IEEE Trans. Acoust. Speech Signal Process.*, vol. 38, no. 5, pp. 814–824, 1990.
- [30] Y. Hua and T. K. Sarkar, “Matrix pencil method and its performance,” in *Int. Conf. on Acoust. Speech Signal Process. (ICASSP)*, IEEE Computer Society, 1988, pp. 2476–2477.
- [31] T. K. Sarkar and O. Pereira, “Using the matrix pencil method to estimate the parameters of a sum of complex exponentials,” *IEEE Antennas Propag. Mag.*, vol. 37, no. 1, pp. 48–55, 1995.
- [32] F. Hu, T. K. Sarkar, and Y. Hua, “Utilization of band-pass filtering for the matrix pencil method,” *IEEE Trans. Signal Process.*, vol. 41, no. 1, pp. 442–442, 1993.
- [33] J. F. del Rio and T. K. Sarkar, “Comparison between the matrix pencil method and the fourier transform technique for high-resolution spectral estimation,” *Digital Signal Process.*, vol. 6, no. 2, pp. 108–125, 1996.
- [34] P. J. Schmid, “Dynamic mode decomposition of numerical and experimental data,” *J. Fluid Mech.*, vol. 656, pp. 5–28, 2010.
- [35] D. Rao, “Perturbation analysis of a svd based method for the harmonic retrieval problem,” in *Int. Conf. on Acoust. Speech Signal Process. (ICASSP)*, IEEE, vol. 10, 1985, pp. 624–627.
- [36] Y. Hua and T. K. Sarkar, “Perturbation analysis of tk method for harmonic retrieval problems,” *IEEE Trans. Acoust. Speech Signal Process.*, vol. 36, no. 2, pp. 228–240, 1988.
- [37] E.-H. Djermoune and M. Tomczak, “Perturbation analysis of subspace-based methods in estimating a damped complex exponential,” *IEEE Trans. Signal Process.*, vol. 57, no. 11, pp. 4558–4563, 2009.
- [38] J. Laroche, “The use of the matrix pencil method for the spectrum analysis of musical signals,” *The Journal of the Acoustical Society of America*, vol. 94, no. 4, pp. 1958–1965, 1993.
- [39] M. Bhuiyan, E. V. Malyarenko, M. A. Pantea, F. M. Seviaryn, and R. G. Maev, “Advantages and limitations of using matrix pencil method for the modal analysis of medical percussion signals,” *IEEE Trans. Biomed. Eng.*, vol. 60, no. 2, pp. 417–426, 2012.
- [40] H. Yin, Z. Zhu, and F. Ding, “Model order determination using the hankel matrix of impulse responses,” *Appl. Math. Lett.*, vol. 24, no. 5, pp. 797–802, 2011.
- [41] P. Stoica and Y. Selen, “Model-order selection: A review of information criterion rules,” *IEEE Signal Process. magazine*, vol. 21, no. 4, pp. 36–47, 2004.
- [42] B. Nadler and A. Kontorovich, “Model selection for sinusoids in noise: Statistical analysis and a new penalty term,” *IEEE Trans. Signal Process.*, vol. 59, no. 4, pp. 1333–1345, 2011.
- [43] J. N. Kutz, S. L. Brunton, B. W. Brunton, and J. L. Proctor, *Dynamic mode decomposition: data-driven modeling of complex systems*. SIAM, 2016.
- [44] J. R. Magnus, “On differentiating eigenvalues and eigenvectors,” *Econom. Theory*, vol. 1, no. 2, pp. 179–191, 1985.
- [45] Y. Katznelson, *An introduction to harmonic analysis*. Cambridge University Press, 2004.
- [46] E. Bronstein, A. Wiegner, D. Shilo, and R. Talmon, “The spatiotemporal coupling in delay-coordinates dynamic mode decomposition,” *Chaos: An Interdisciplinary Journal of Nonlinear Science*, vol. 32, no. 12, p. 123127, 2022.
- [47] Y. Hua and T. K. Sarkar, “On svd for estimating generalized eigenvalues of singular matrix pencil in noise,” in *1991, IEEE Int. Symposium on Circuits and Syst.*, IEEE, 1991, pp. 2780–2783.
- [48] O. Roy and M. Vetterli, “The effective rank: A measure of effective dimensionality,” in *2007 15th European signal process. conf.*, IEEE, 2007, pp. 606–610.
- [49] S. Dharanipragada and K. Arun, “Resolution limits in signal recovery,” *IEEE Trans. Signal Process.*, vol. 44, no. 3, pp. 546–561, 1996.
- [50] M. Shahram and P. Milanfar, “On the resolvability of sinusoids with nearby frequencies in the presence of noise,” *IEEE Trans. Signal Process.*, vol. 53, no. 7, pp. 2579–2588, 2005.
- [51] A. Amar and A. J. Weiss, “Fundamental limitations on the resolution of deterministic signals,” *IEEE Trans. Signal Process.*, vol. 56, no. 11, pp. 5309–5318, 2008.
- [52] R. Kumaresan and D. Tufts, “Estimating the parameters of exponentially damped sinusoids and pole-zero modeling in noise,” *IEEE Trans. Acoust. Speech Signal Process.*, vol. 30, no. 6, pp. 833–840, 1982.
- [53] S.-Y. Kung, K. S. Arun, and D. B. Rao, “State-space and singular-value decomposition-based approximation methods for the harmonic retrieval problem,” *JOSA*, vol. 73, no. 12, pp. 1799–1811, 1983.
- [54] D. S. Broomhead and G. P. King, “Extracting qualitative dynamics from experimental data,” *Physica D*, vol. 20, no. 2-3, pp. 217–236, 1986.
- [55] J. B. Elsner and A. A. Tsonis, *Singular spectrum analysis: a new tool in time series analysis*. Springer Science & Business Media, 1996.

Structure-Aware Matrix Pencil Method

Supplementary Materials

Yehonatan-Itay Segman, Alon Amar, and Ronen Talmon, *Senior Member, IEEE*

APPENDIX A SIMPLE EIGENVECTOR PERTURBATION

In this appendix, we derive a first-order approximation for a simple eigenvector under perturbation. Simple eigenvectors, associated with simple eigenvalues, are known to display stable behavior under perturbations [1, 2]. Following [1], let $\mathbf{A} \in \mathbb{C}^{n \times n}$ be a complex square matrix, and let \mathbf{v}_i denote a simple right eigenvector of \mathbf{A} corresponding to a simple eigenvalue λ_i . For a perturbed matrix $\mathbf{A} + \delta\mathbf{A}$, the author established the existence of a complex function λ and a complex vector function \mathbf{v} defined for all $\delta\mathbf{A}$ in a neighborhood of \mathbf{A} , satisfying $\lambda(\mathbf{A}) = \lambda_i$, $\mathbf{v}(\mathbf{A}) = \mathbf{v}_i$, and $(\mathbf{A} + \delta\mathbf{A})\mathbf{v} = \lambda\mathbf{v}$. These functions are infinitely differentiable within this neighborhood, with their differentials at \mathbf{A} also provided. While the proof is clear and elegant, we seek an alternative proof that will provide additional insights into the neighborhood in which eigenvector perturbation can be characterized.

Our approach follows the technique outlined in [3, Theorem 4.1], which assumes that the matrix \mathbf{A} is non-defective, forming an eigenvector basis for \mathbb{C}^n . Let \mathbf{V} and \mathbf{U} denote the matrices of its right and left eigenvectors, respectively, where \mathbf{u}_k^H is the k -th row of \mathbf{U}^H and \mathbf{v}_i is the i -th column of \mathbf{V} . The following lemma characterizes the approximate behavior of \mathbf{v}_i under perturbation, provided that a delicate balance between perturbation and eigenvalue separation is maintained.

Lemma 1. *Let \mathbf{v}_i be a simple right eigenvector of a non-defective matrix $\mathbf{A} \in \mathbb{C}^{n \times n}$, and let λ_i be its associated to simple eigenvalue. Then there is a unique right eigenvector $\tilde{\mathbf{v}}_i = \mathbf{v}_i + \delta\mathbf{v}_i$ of the matrix $\mathbf{A} + \delta\mathbf{A}$ and a corresponding eigenvalue $\tilde{\lambda}_i = \lambda_i + \delta\lambda_i$ such that $\delta\lambda_i$ and $\delta\mathbf{v}_i$ can be approximated to first order by*

$$\delta\lambda_i = \frac{\mathbf{u}_i^H \delta\mathbf{A} \mathbf{v}_i}{\mathbf{u}_i^H \mathbf{v}_i}, \quad (47)$$

$$\delta\mathbf{v}_i = \sum_{k=1, k \neq i}^n \frac{\mathbf{u}_k^H \delta\mathbf{A} \mathbf{v}_i}{\mathbf{u}_k^H \mathbf{v}_k (\tilde{\lambda}_i - \lambda_k)} \mathbf{v}_k. \quad (48)$$

Provided that

$$\rho(\mathbf{D}_i \mathbf{U}^H \delta\mathbf{A} \mathbf{V}) < 1, \quad (49)$$

and

$$\mathbf{u}_i^H \mathbf{v}_i = 1, \quad \mathbf{u}_i^H \tilde{\mathbf{v}}_i = 1, \quad (50)$$

The authors are with the Viterbi Faculty of Electrical and Computer Engineering, Technion – Israel Institute of Technology, Haifa 32000, Israel. (Corresponding author: Yehonatan-Itay Segman, email: yehonatans@campus.technion.ac.il).

where $\rho(\cdot)$ is the spectral radius, and the matrix \mathbf{D}_i is a diagonal matrix defined by

$$\mathbf{D}_i = \text{diag}\left(\frac{1}{\mathbf{u}_1^H \mathbf{v}_1 (\tilde{\lambda}_i - \lambda_1)}, \dots, 0_i, \dots, \frac{1}{\mathbf{u}_n^H \mathbf{v}_n (\tilde{\lambda}_i - \lambda_n)}\right). \quad (51)$$

Proof. The fact that there is a unique perturbed eigenvalue $\tilde{\lambda}_i$ such that

$$\delta\lambda_i = \frac{\mathbf{u}_i^H \delta\mathbf{A} \mathbf{v}_i}{\mathbf{u}_i^H \mathbf{v}_i} + O(\|\delta\mathbf{A}\|^2), \quad (52)$$

is provided in [4, chapter IV, Theorem 2.3]. Let $\tilde{\mathbf{v}}_i$ be its corresponding perturbed eigenvector. The non-defectiveness of the matrix \mathbf{A} implies that we can expand $\delta\mathbf{v}_i = \tilde{\mathbf{v}}_i - \mathbf{v}_i$ in the eigenvector basis of \mathbf{A} as:

$$\delta\mathbf{v}_i = \sum_{k=1}^n a_{ik} \mathbf{v}_k. \quad (53)$$

Left multiplying (53) by \mathbf{u}_i^H results in:

$$a_{ii} = \frac{\mathbf{u}_i^H \tilde{\mathbf{v}}_i - \mathbf{u}_i^H \mathbf{v}_i}{\mathbf{u}_i^H \mathbf{v}_i}. \quad (54)$$

It follows, by assumption (50), that $a_{ii} = 0$. Thus, (53) can be written as:

$$\delta\mathbf{v}_i = \sum_{\substack{k=1 \\ k \neq i}}^n a_{ik} \mathbf{v}_k. \quad (55)$$

It is noteworthy that as the matrix \mathbf{A} is non-defective, its right eigenvector matrix \mathbf{V} , is invertible. As eigenvectors are unique up to scalar multiplication, it follows that there exists a diagonal matrix $\mathbf{C} = \text{diag}(c_1, \dots, c_n)$, where $\{c_k\}_{k=1}^n \neq 0$, such that $\mathbf{C}\mathbf{V}^{-1} = \mathbf{U}^H$ or equivalently $\mathbf{C} = \mathbf{U}^H \mathbf{V}$. Consequently, each element c_k can be expressed as $c_k = \mathbf{u}_k^H \mathbf{v}_k$, ensuring that all the terms involving the reciprocal of $\mathbf{u}_i^H \mathbf{v}_i$ are well defined.

The perturbed eigenvalue problem can be stated as

$$(\mathbf{A} + \delta\mathbf{A})(\mathbf{v}_i + \delta\mathbf{v}_i) = (\lambda_i + \delta\lambda_i)(\mathbf{v}_i + \delta\mathbf{v}_i).$$

Left multiplying by \mathbf{u}_k^H for $k \neq i$ and rearranging, we can express the vector of coefficients \mathbf{a}_i , from (55), by the following relation:

$$(\mathbf{I} - \mathbf{D}_i \mathbf{U}^H \delta\mathbf{A} \mathbf{T}) \mathbf{a}_i = \mathbf{D}_i \mathbf{U}^H \delta\mathbf{A} \mathbf{v}_i, \quad (56)$$

where the matrix \mathbf{D}_i is defined in (51).

By Assumption (49), the spectral radius $\rho(\mathbf{D}_i \mathbf{U}^H \delta\mathbf{A} \mathbf{V}) < 1$, and we can explicitly express the coefficients vector \mathbf{a}_i by inverting the matrix $(\mathbf{I} - \mathbf{D}_i \mathbf{U}^H \delta\mathbf{A} \mathbf{V})$. Finally, as $\rho(\mathbf{D}_i \mathbf{U}^H \delta\mathbf{A} \mathbf{V}) < 1$, using the Neumann series representation

of the matrix $(\mathbf{I} - \mathbf{D}_i \mathbf{U}^H \delta \mathbf{A} \mathbf{V})^{-1}$, we get the following first-order approximation for the coefficients vector:

$$\mathbf{a}_i = \mathbf{D}_i \mathbf{U}^H \delta \mathbf{A} \mathbf{v}_i. \quad (57)$$

This leads us to the following expression for a_{ik} :

$$a_{ik} = \begin{cases} 0 & , \text{if } k = i, \\ \frac{\mathbf{u}_k^H \delta \mathbf{A} \mathbf{v}_i}{\mathbf{u}_k^H \mathbf{v}_k (\lambda_i - \lambda_k)} & , \text{otherwise} \end{cases} \quad (58)$$

which completes the proof. \square

APPENDIX B EXTENDING THE MATRIX PENCIL THEOREM: ACCOUNTING FOR NOISE EFFECTS

In this section, we extend the MP theorem [5, Theorem 2.1] to the noisy case and analyze the noise-induced effects. By doing so, we bridge the gap between the existing theory, described in Section II-C, and practice, described in Section II-A.

Theorem 1. Assume the underlying signal is given by (1). Let \mathbf{Y}_0 and \mathbf{Y}_1 be the Hankel matrices defined in (3). Then, \mathbf{Y}_0 and \mathbf{Y}_1 admit the following factorization:

$$\mathbf{Y}_0 = \tilde{\mathbf{Z}}_L \tilde{\mathbf{B}} \tilde{\mathbf{Z}}_R, \quad (59)$$

$$\mathbf{Y}_1 = \tilde{\mathbf{Z}}_L \tilde{\mathbf{B}} \tilde{\Lambda} \tilde{\mathbf{Z}}_R, \quad (60)$$

where

- 1) The diagonal matrix $\tilde{\Lambda}$ consists of the MP eigenvalues, acts as a forward propagation in time, and can be recast as:

$$\tilde{\Lambda} = \begin{bmatrix} \tilde{\mathbf{Z}} & 0 \\ 0 & \tilde{\mathbf{0}} \end{bmatrix}_{L \times L}, \quad (61)$$

where

- a) The diagonal matrix $\tilde{\mathbf{Z}} \in \mathbb{C}^{M \times M}$ comprises the signal-related eigenvalues.
- b) The diagonal matrix $\tilde{\mathbf{0}} \in \mathbb{C}^{(L-M) \times (L-M)}$ consists of the noise-related eigenvalues.
- 2) The diagonal matrix $\tilde{\mathbf{B}}$ can be cast as

$$\tilde{\mathbf{B}} = \begin{bmatrix} \mathbf{B} & 0 \\ 0 & \mathbf{I}_{L-M} \end{bmatrix}_{L \times L}, \quad (62)$$

where the diagonal matrix $\mathbf{B} \in \mathbb{C}^{M \times M}$ consists of the signal amplitudes as defined in 17.

- 3) $\tilde{\mathbf{Z}}_R$, which is defined in (18) as the pseudo-inverse of the right eigenvector matrix of the noisy MP, can be recast as:

$$\tilde{\mathbf{Z}}_R = \begin{bmatrix} \mathbf{Z}_R + \mathbf{E}_R \\ \mathbf{C}_R \end{bmatrix}_{L \times L}, \quad (63)$$

where the top M rows of $\tilde{\mathbf{Z}}_R$ are the sum of the Vandermonde matrix \mathbf{Z}_R and a noise-related component, denoted by \mathbf{E}_R . The remaining $L - M$ rows are noise-related spurious rows, denoted by \mathbf{C}_R .

- 4) $\tilde{\mathbf{Z}}_L$, which is defined in (19) as the pseudo-inverse of the left eigenvector matrix of the noisy MP, can be recast as

$$\tilde{\mathbf{Z}}_L = [\mathbf{Z}_L + \mathbf{E}_L, \mathbf{C}_L]_{(N-L) \times L}, \quad (64)$$

where the leftmost M columns of $\tilde{\mathbf{Z}}_L$ are the sum of the Vandermonde matrix \mathbf{Z}_L and a noise-related component, denoted by \mathbf{E}_L . The remaining $L - M$ columns are noise-related spurious columns, denoted by \mathbf{C}_L .

Proof. Using the definition of $\tilde{\mathbf{Z}}_R^\dagger$ and $\tilde{\mathbf{Z}}_L^\dagger$ from (20) and (21), and the SVD of $\mathbf{Y}_0 = \mathbf{U} \Sigma \mathbf{V}^H$ from (4), it is easy to verify that $\tilde{\mathbf{Z}}_L^\dagger \mathbf{Y}_0 \tilde{\mathbf{Z}}_R^\dagger = \mathbf{I}_L$, and $\tilde{\mathbf{Z}}_L^\dagger \mathbf{Y}_1 \tilde{\mathbf{Z}}_R^\dagger = \tilde{\Lambda}$, where \mathbf{I}_L is the $L \times L$ identity matrix. From these equalities we find a new representation for the noisy Hankel matrices:

$$\mathbf{Y}_0 = \tilde{\mathbf{Z}}_L \tilde{\mathbf{Z}}_R, \quad (65)$$

$$\mathbf{Y}_1 = \tilde{\mathbf{Z}}_L \tilde{\Lambda} \tilde{\mathbf{Z}}_R. \quad (66)$$

By employing the Vandermonde factorization of \mathbf{X}_0 , we can express the Hankel matrix \mathbf{Y}_0 as

$$\mathbf{Y}_0 = \mathbf{X}_0 + \mathbf{W}_0 = \mathbf{Z}_L \mathbf{B} \mathbf{Z}_R + \mathbf{W}_0. \quad (67)$$

Let us re-frame equation (67) as follows:

$$\mathbf{Y}_0 = (\mathbf{Z}_L \mathbf{B}^{\frac{1}{2}})(\mathbf{B}^{\frac{1}{2}} \mathbf{Z}_R) + \mathbf{W}_0, \quad (68)$$

as this formulation will prove to be useful in subsequent discussions. Combining (65) and (68), we get:

$$\tilde{\mathbf{Z}}_L = (\mathbf{Z}_L \mathbf{B}^{\frac{1}{2}})(\mathbf{B}^{\frac{1}{2}} \mathbf{Z}_R) \tilde{\mathbf{Z}}_R^\dagger + \mathbf{W}_0 \tilde{\mathbf{Z}}_R^\dagger. \quad (69)$$

Now, let us analyze the term $\mathbf{B}^{\frac{1}{2}} \mathbf{Z}_R \tilde{\mathbf{Z}}_R^\dagger$. As established in [5, Theorem 2.1], the columns of \mathbf{Z}_R^\dagger (and hence the columns of $\mathbf{Z}_R^\dagger \mathbf{B}^{-\frac{1}{2}}$) are right eigenvectors of the noiseless MP $(\mathbf{X}_0, \mathbf{X}_1)$, or equivalently, right simple eigenvectors of $\mathbf{X}_0^\dagger \mathbf{X}_1$ corresponding to its non-zero and simple eigenvalues. Furthermore, by definition, the columns of $\tilde{\mathbf{Z}}_R^\dagger$ are right eigenvectors of the noisy MP $\mathbf{Y}_1 - \lambda \mathbf{Y}_0$, or equivalently, right eigenvectors of $\mathbf{Y}_0^\dagger \mathbf{Y}_1$.

As each $\{z_i\}_{i=1}^M$ is a simple eigenvalue of $\mathbf{X}_0^\dagger \mathbf{X}_1$, and $\mathbf{Y}_0^\dagger \mathbf{Y}_1$ is a perturbation of $\mathbf{X}_0^\dagger \mathbf{X}_1$, according to Theorem 2.3, chapter IV in [4], we can uniquely match each simple eigenvector of $\mathbf{X}_0^\dagger \mathbf{X}_1$ with a simple eigenvector of $\mathbf{Y}_0^\dagger \mathbf{Y}_1$ ¹. Without loss of generality, let the leftmost M columns of $\tilde{\mathbf{Z}}_R^\dagger$ consist of these perturbed eigenvectors, which are the M columns of \mathbf{Z}_R^\dagger . Consequently, we can express this relationship as follows:

$$\tilde{\mathbf{Z}}_R^\dagger = [\mathbf{Z}_R^\dagger \mathbf{B}^{-\frac{1}{2}} + \delta \mathbf{Z}_R^\dagger, \mathbf{C}_1]_{L \times L} \quad (70)$$

where $\mathbf{C}_1 \in \mathbb{C}^{L \times (L-M)}$ contains the remaining $L - M$ eigenvectors of $\mathbf{Y}_0^\dagger \mathbf{Y}_1$ and $\delta \mathbf{Z}_R^\dagger \in \mathbb{C}^{L \times M}$ represents the additive discrepancy in the scaled, right eigenvectors matrix $\mathbf{Z}_R^\dagger \mathbf{B}^{-\frac{1}{2}}$ due to the perturbation of the noiseless matrix $\mathbf{X}_0^\dagger \mathbf{X}_1$. Substituting (70) into (69), we get the following structure of the left mode:

¹Theorem 2.3, chapter IV in [4] guarantees that there is a unique perturbed eigenvalue \tilde{z}_i , such that

$$\tilde{z}_i = z_i + \frac{\mathbf{p}_i'^* \delta(\mathbf{X}_0^\dagger \mathbf{X}_1) \mathbf{q}_i'}{\mathbf{p}_i'^* \mathbf{q}_i'} + O(\|\delta(\mathbf{X}_0^\dagger \mathbf{X}_1)\|^2)$$

where \mathbf{q}_i' and $\mathbf{p}_i'^*$ are the corresponding right and left eigenvectors of the matrix $\mathbf{X}_0^\dagger \mathbf{X}_1$ and $\mathbf{Y}_0^\dagger \mathbf{Y}_1 = \mathbf{X}_0^\dagger \mathbf{X}_1 + \delta(\mathbf{X}_0^\dagger \mathbf{X}_1)$.

$$\begin{aligned} \tilde{\mathbf{Z}}_L &= (\mathbf{Z}_L \mathbf{B}^{\frac{1}{2}})(\mathbf{B}^{\frac{1}{2}} \mathbf{Z}_R) [\mathbf{Z}_R^\dagger \mathbf{B}^{-\frac{1}{2}} + \delta \mathbf{Z}_R^\dagger, \mathbf{C}_1] + \\ &\quad \mathbf{W}_0 [\mathbf{Z}_R^\dagger \mathbf{B}^{-\frac{1}{2}} + \delta \mathbf{Z}_R^\dagger, \mathbf{C}_1]. \end{aligned} \quad (71)$$

Which can be re-arranged to the following form:

$$\tilde{\mathbf{Z}}_L = [\mathbf{Z}_L \mathbf{B}^{\frac{1}{2}} + \mathbf{X}_0 \delta \mathbf{Z}_R^\dagger + \mathbf{W}_0 \mathbf{Z}_R^\dagger \mathbf{B}^{-\frac{1}{2}} + \mathbf{W}_0 \delta \mathbf{Z}_R^\dagger, \mathbf{Y}_0 \mathbf{C}_1]. \quad (72)$$

To obtain the desired normalized form, define the diagonal matrix

$$\tilde{\mathbf{B}} = \begin{bmatrix} \mathbf{B} & 0 \\ 0 & \mathbf{I}_{L-M} \end{bmatrix}_{L \times L},$$

to get

$$\tilde{\mathbf{Z}}_L \tilde{\mathbf{B}}^{-\frac{1}{2}} = [\mathbf{Z}_L + \mathbf{E}_L, \mathbf{C}_L], \quad (73)$$

where the noise-related component \mathbf{E}_L and the spurious matrix \mathbf{C}_L are defined by

$$\mathbf{E}_L = \mathbf{X}_0 \delta \mathbf{Z}_R^\dagger \mathbf{B}^{-\frac{1}{2}} + \mathbf{W}_0 \mathbf{Z}_R^\dagger \mathbf{B}^{-1} + \mathbf{W}_0 \delta \mathbf{Z}_R^\dagger \mathbf{B}^{-\frac{1}{2}}, \quad (74)$$

$$\mathbf{C}_L = \mathbf{Y}_0 \mathbf{C}_1. \quad (75)$$

For simplicity, we maintain the notation $\tilde{\mathbf{Z}}_L$ for the normalized form, i.e., $\tilde{\mathbf{Z}}_L = \tilde{\mathbf{Z}}_L \tilde{\mathbf{B}}^{-\frac{1}{2}}$.

Following the same technique as in (70), the left eigenvectors matrix can be recast as:

$$\tilde{\mathbf{Z}}_L^\dagger = \begin{bmatrix} \mathbf{B}^{-\frac{1}{2}} \mathbf{Z}_L^\dagger + \delta \mathbf{Z}_L^\dagger \\ \mathbf{C}_2 \end{bmatrix}_{L \times (N-L)}, \quad (76)$$

where $\mathbf{C}_2 \in \mathbb{C}^{(L-M) \times (N-L)}$ and $\delta \mathbf{Z}_L^\dagger \in \mathbb{C}^{M \times (N-L)}$, to obtain the desired structure of:

$$\tilde{\mathbf{B}}^{-\frac{1}{2}} \tilde{\mathbf{Z}}_R = \begin{bmatrix} \mathbf{Z}_R + \mathbf{E}_R \\ \mathbf{C}_R \end{bmatrix}, \quad (77)$$

where,

$$\mathbf{E}_R = \mathbf{B}^{-\frac{1}{2}} \delta \mathbf{Z}_L^\dagger \mathbf{X}_0 + \mathbf{B}^{-1} \mathbf{Z}_L^\dagger \mathbf{W}_0 + \mathbf{B}^{-\frac{1}{2}} \delta \mathbf{Z}_L^\dagger \mathbf{W}_0, \quad (78)$$

$$\mathbf{C}_R = \mathbf{C}_2 \mathbf{Y}_0. \quad (79)$$

For simplicity, we maintain the notation $\tilde{\mathbf{Z}}_R$ for the normalized form, i.e., $\tilde{\mathbf{Z}}_R = \tilde{\mathbf{B}}^{-\frac{1}{2}} \tilde{\mathbf{Z}}_L$. Combining the normalized forms of $\tilde{\mathbf{Z}}_L$ and $\tilde{\mathbf{Z}}_R$ with the decomposition of the Hankel matrices \mathbf{Y}_0 and \mathbf{Y}_1 from (65) and (66) leads to the desired normalized factorization of $\mathbf{Y}_0 = \tilde{\mathbf{Z}}_L \tilde{\mathbf{B}} \tilde{\mathbf{Z}}_R$ and $\mathbf{Y}_1 = \tilde{\mathbf{Z}}_L \tilde{\mathbf{B}} \tilde{\Lambda} \tilde{\mathbf{Z}}_R$.

The partitioning of $\tilde{\Lambda}$ to signal-related and noise-related components is derived from the assumption on the order of vectors in $\tilde{\mathbf{Z}}_R^\dagger$ and $\tilde{\mathbf{Z}}_L^\dagger$. We assumed, without loss of generality, that the leftmost M columns of $\tilde{\mathbf{Z}}_R^\dagger$ are the perturbed versions of the M simple right eigenvectors of $\mathbf{X}_0^\dagger \mathbf{X}_1$ corresponding to the signal poles. A parallel assumption is made on the top M rows of $\tilde{\mathbf{Z}}_L^\dagger$. Such ordering, of the right and left eigenvectors of the matrix $\mathbf{X}_0^\dagger \mathbf{X}_1$, induces the same ordering on the corresponding eigenvalues matrix $\tilde{\Lambda}$. Hence the decomposition of $\tilde{\Lambda}$ in (61). This completes the proof. \square

APPENDIX C PROOF OF PROPOSITION 2

Proof. The left additive error term was shown to be:

$$\mathbf{E}_L = \mathbf{X}_0 \delta \mathbf{Z}_R^\dagger \mathbf{B}^{-\frac{1}{2}} + \mathbf{W}_0 \mathbf{Z}_R^\dagger \mathbf{B}^{-1} + \mathbf{W}_0 \delta \mathbf{Z}_R^\dagger \mathbf{B}^{-\frac{1}{2}}. \quad (80)$$

We begin by examining the term $\delta \mathbf{Z}_R^\dagger \in \mathbb{C}^{L \times M}$, which represents the additive discrepancy in the scaled right eigenvectors matrix of the noiseless MP pair $(\mathbf{X}_0, \mathbf{X}_1)$. Recalling that the matrix $\mathbf{X}_0^\dagger \mathbf{X}_1$ is non-defective, with its complete set of L independent right and left eigenvectors denoted as $\{\mathbf{q}_k'\}_{k=1}^L$ and $\{\mathbf{p}_k'\}_{k=1}^L$, respectively. Let $\{\delta \mathbf{q}_i\}_{i=1}^M$ represent the i -th column of $\delta \mathbf{Z}_R^\dagger$. We can express $\delta \mathbf{q}_i$ as:

$$\delta \mathbf{q}_i = \sum_{k=1}^L a_{ik} \mathbf{q}_k' = \sum_{k=1}^M a_{ik} \mathbf{q}_k' + \sum_{k=M+1}^L a_{ik} \mathbf{q}_k'. \quad (81)$$

Through the Vandermonde factorization of \mathbf{X}_0 and \mathbf{X}_1 , we get $\mathbf{X}_0^\dagger \mathbf{X}_1 = \mathbf{Z}_R^\dagger \mathbf{Z}_R$. Consequently, for $1 \leq k \leq M$ \mathbf{q}_k' is the k -th column of \mathbf{Z}_R^\dagger , $\mathbf{p}_k'^H$ is the k -th row of \mathbf{Z}_R and $\mathbf{p}_k'^H \mathbf{q}_k' = 1$. It follows from Theorem [5, Theorem 2.1] that $\mathbf{q}_k' = \mathbf{q}_k$ for $1 \leq k \leq M$. However, for $M < k \leq L$, \mathbf{q}_k' lies in the null space of $\mathbf{X}_0^\dagger \mathbf{X}_1$, implying $\mathbf{X}_0 \mathbf{q}_k' = 0$. Substituting this decomposition back into (80), we obtain:

$$\mathbf{E}_L^i = \frac{\mathbf{X}_0}{\sqrt{b_i}} \sum_{k=1}^M a_{ik} \mathbf{q}_k + \frac{\mathbf{W}_0 \mathbf{q}_i}{b_i} + \frac{\mathbf{W}_0}{\sqrt{b_i}} \sum_{k=1}^L a_{ik} \mathbf{q}_k'. \quad (82)$$

Using again the Vandermonde factorization of $\mathbf{X}_0 = \mathbf{Z}_L \mathbf{B} \mathbf{Z}_R$ and the fact that \mathbf{q}_k is the k -th column of \mathbf{Z}_R^\dagger , we get:

$$\mathbf{E}_L^i = \sum_{k=1}^M \frac{a_{ik} b_k}{\sqrt{b_i}} \begin{bmatrix} 1 \\ z_k \\ \vdots \\ z_k^{N-L-1} \end{bmatrix} + \frac{\mathbf{W}_0 \mathbf{q}_i}{b_i} + \frac{\mathbf{W}_0}{\sqrt{b_i}} \sum_{k=1}^L a_{ik} \mathbf{q}_k'. \quad (83)$$

We now turn to get a first-order approximation of the coefficients a_{ik} using Lemma 1 applied to the matrix $\mathbf{X}_0^\dagger \mathbf{X}_1$, its perturbation $\mathbf{Y}_0^\dagger \mathbf{Y}_1 = \mathbf{X}_0^\dagger \mathbf{X}_1 + \delta(\mathbf{X}_0^\dagger \mathbf{X}_1)$, and to the simple, scaled, right eigenvectors $\mathbf{Z}_R^\dagger \mathbf{B}^{-\frac{1}{2}}$ of $\mathbf{X}_0^\dagger \mathbf{X}_1$.

Lemma 1 assumes a specific normalization for the right, simple eigenvectors, and their perturbation. As noted above, for each simple eigenvector $\{\mathbf{q}_k'\}_{k=1}^M$ it holds that $\mathbf{p}_k'^H \mathbf{q}_k' = 1$. Additionally, by our Assumption 1, we have $\mathbf{p}_k'^H \tilde{\mathbf{q}}_k' = 1$. Finally, by Assumption (26), $\rho(\mathbf{D}_i \mathbf{T}_L \delta(\mathbf{X}_0^\dagger \mathbf{X}_1) \mathbf{T}_R) < 1$, and hence we can apply Lemma 1 to get the first order approximation of the coefficients a_{ik} :

$$a_{ik} = \begin{cases} 0 & , k = i \\ \frac{\mathbf{p}_k'^H \delta(\mathbf{X}_0^\dagger \mathbf{X}_1) \mathbf{q}_i'}{\sqrt{b_i}(\lambda_i - \lambda_k)} & , \text{otherwise.} \end{cases}$$

Note that λ_k are the eigenvalues of $\mathbf{X}_0^\dagger \mathbf{X}_1$, which are assumed to be indexed such that:

$$\lambda_k = \begin{cases} z_k, & \text{if } 1 \leq k \leq M \\ 0, & \text{otherwise,} \end{cases}$$

and $\tilde{\lambda}_i$ is the unique perturbation of λ_i as described in Lemma 1. As noted above, $\mathbf{q}'_i = \mathbf{q}_i$ for $1 \leq i \leq M$ and hence:

$$a_{ik} = \begin{cases} 0 & , k = i \\ \frac{\mathbf{p}'_k^H \delta(\mathbf{X}_0^\dagger \mathbf{X}_1) \mathbf{q}_i}{\sqrt{b_i}(\tilde{\lambda}_i - \lambda_k)} & , \text{otherwise.} \end{cases}$$

Following the approach presented in [5, section IV], the term $\mathbf{p}'_k^H \delta(\mathbf{X}_0^\dagger \mathbf{X}_1) \mathbf{q}_i$, can be approximated to first order by

$$\mathbf{p}'_k^H \delta(\mathbf{X}_0^\dagger \mathbf{X}_1) \mathbf{q}_i = \mathbf{p}'_k^H (\delta(\mathbf{Y}_0^\dagger) \mathbf{X}_1) \mathbf{q}_i + \mathbf{p}'_k^H (\mathbf{X}_0^\dagger \mathbf{W}_1) \mathbf{q}_i. \quad (84)$$

For $1 \leq k \leq M$ it is also shown in [5] that a first order approximation of (84) is given by:

$$\mathbf{p}'_k^H \delta(\mathbf{X}_0^\dagger \mathbf{X}_1) \mathbf{q}_i = \frac{\mathbf{p}_k^H (\mathbf{W}_1 - z_i \mathbf{W}_0) \mathbf{q}_i}{b_i}, \quad (85)$$

where \mathbf{p}_k^H is the k -th row of \mathbf{Z}_L^\dagger , as described in [5, Theorem 2.1]. On the other hand, for $M < k \leq L$, the rightmost term of (84) annihilates and we are left with $\mathbf{p}_k^H (\delta(\mathbf{Y}_0^\dagger) \mathbf{X}_1) \mathbf{q}_i$. Using the decomposition theorem for pseudo-inverses, given in [6], we can write:

$$\begin{aligned} \delta \mathbf{Y}_0^\dagger &= -\mathbf{Y}_0^\dagger \mathbf{W}_0 \mathbf{X}_0^\dagger + (\mathbf{Y}_0^\dagger \mathbf{Y}_0)^\dagger \mathbf{W}_0^H P_{N(\mathbf{X}_0^H)} \\ &\quad + P_{N(\mathbf{Y}_0)} \mathbf{W}_0^H (\mathbf{X}_0 \mathbf{X}_0^H)^\dagger, \end{aligned} \quad (86)$$

where P_X is the orthogonal projection onto a subspace X .

Combining (85) and (86) back into (83), a first order approximation of \mathbf{E}_L^i is given by:

$$\mathbf{E}_L^i = \sum_{\substack{k=1 \\ k \neq i}}^M \frac{\mathbf{p}_k^H (\mathbf{W}_1 - z_i \mathbf{W}_0) \mathbf{q}_i}{b_i(\tilde{\lambda}_i - z_k)} \begin{bmatrix} 1 \\ z_k \\ \vdots \\ z_k^{N-L-1} \end{bmatrix} + \frac{\mathbf{W}_0 \mathbf{q}_i}{b_i}. \quad (87)$$

□

Remark 6. Assumption (26) intricately implies a delicate balance between the i -th pole separation and perturbation. Two observations support this. (i) Recognizing that matrix \mathbf{D}_i contains information about the separation and perturbation of the i -th pole as:

$$(\tilde{\lambda}_i - \lambda_k) = (\tilde{\lambda}_i - \lambda_i) - (\lambda_k - \lambda_i).$$

(ii) Referring to [4, Theorem 3.3, Chapter IV], the following inequality holds:

$$\max_i \min_k |\tilde{\lambda}_i - \lambda_k| \leq \|\mathbf{T}_R^{-1} \delta(\mathbf{X}_0^\dagger \mathbf{X}_1) \mathbf{T}_R\|, \quad (88)$$

and hence the inequality:

$$1 \leq \frac{\|\mathbf{T}_R^{-1} \delta(\mathbf{X}_0^\dagger \mathbf{X}_1) \mathbf{T}_R\|}{\min_k |\tilde{\lambda}_i - \lambda_k|} \quad (89)$$

holds for all indices $1 \leq i \leq M$.

Equations (26) and (89) are related through the connection between the spectral radius and spectral norm, but differ in two aspects: (i) the i -th coordinate of the matrix \mathbf{D}_i is set to zero², and (ii) the matrix norm is used, providing a natural upper bound on the spectral radius.

²This motivates the eigenvector normalization in Assumption 1.

APPENDIX D PROOF OF PROPOSITION 3

Proof. Recall that:

$$\gamma_{i,m} = \frac{\mathbf{u}_m^T \mathbf{Q}_i \mathbf{w}}{(\tilde{\lambda}_i - z_m) b_i}, \quad \xi_i = \frac{\mathbf{I}_0 \mathbf{Q}_i \mathbf{w}}{b_i}, \quad (90)$$

and for simplicity, denote:

$$\bar{\gamma}_{i,m} = \frac{\mathbf{u}_m^T \mathbf{Q}_i \mathbf{w}}{b_i}. \quad (91)$$

Equation (90) shows that $\bar{\gamma}_{i,m}$ and the entries of ξ_i are a linear combination of the complex, i.i.d Gaussian random variables $\{\mathbf{w}(n)\}_{n=1}^n$ with zero mean and variance σ_w^2 . Hence, $\bar{\gamma}_{i,m}$ and the entries of ξ_i are also complex, Gaussian random variables with zero mean. Inspecting the circular structure of the matrix \mathbf{Q}_i , we can recast the term $\mathbf{u}_m \mathbf{Q}_i$ as the convolution of the vectors \mathbf{q}_i and \mathbf{u}_m . Using (91), we derive the following statistics of $\bar{\gamma}_{i,m}$:

$$\mathbb{E}[\bar{\gamma}_{i,m}] = 0, \quad (92)$$

$$\text{Var}(\bar{\gamma}_{i,m}) = \frac{\|\mathbf{u}_m * \mathbf{q}_i\|_2^2}{\text{SNR}_i}. \quad (93)$$

It is worth recalling that the vector \mathbf{u}_m was defined in (32) by

$$\mathbf{u}_m^T = [0, \mathbf{p}_m^H] - z_i [\mathbf{p}_m^H, 0],$$

where \mathbf{p}_m^H and \mathbf{q}_i depend solely on the signal poles and the parameters N and L , as they are also given by the m -th row of \mathbf{Z}_L^\dagger and i -th column of \mathbf{Z}_R^\dagger , respectively.

Since $\bar{\gamma}_{i,m}$ is a complex Gaussian random variable, $|\bar{\gamma}_{i,m}|$ follows a Rayleigh distribution with scale parameter $\sigma_{\bar{\gamma}_{i,m}} = \text{var}(\bar{\gamma}_{i,m})$. By setting $t = \sigma_{\bar{\gamma}_{i,m}} \sqrt{2 \log(\frac{1}{\varepsilon})}$, we ensure that $|\bar{\gamma}_{i,m}| \leq t$ with a probability of at least $1 - \varepsilon$. Utilizing (93), it follows that:

$$|\bar{\gamma}_{i,m}| \leq \sqrt{\frac{2 \log(\frac{1}{\varepsilon})}{\text{SNR}_i}} \|\mathbf{u}_m * \mathbf{q}_i\|_2,$$

with a probability of at least $1 - \varepsilon$.

To derive the bound on $\gamma_{i,m}$, we use our assumption that $|z_i - z_m| \geq 2|\delta z_i|$ for $m \neq i$, to get:

$$|\tilde{\lambda}_i - z_m| = |z_i + \delta z_i - z_m| \geq |z_i - z_m| - |\delta z_i| \geq \frac{|z_i - z_m|}{2}.$$

Finally, we derive that:

$$|\gamma_{i,m}| \leq 2 \sqrt{\frac{2 \log(\frac{1}{\varepsilon})}{\text{SNR}_i}} \frac{\|\mathbf{u}_m * \mathbf{q}_i\|_2}{|z_i - z_m|},$$

with a probability of at least $1 - \varepsilon$.

The entries of ξ_i can be bounded similarly. Writing the k -th entry of ξ_i by $\xi_i(k) = \mathbf{e}_k^T \xi_i$, where \mathbf{e}_k is the k -th standard unit vector we get:

$$\xi_i(k) = \frac{\mathbf{e}_k^T \mathbf{I}_0 \mathbf{Q}_i \mathbf{w}}{b_i},$$

and we derive the following statistics of $\xi_i(k)$:

$$\mathbb{E}[\xi_i(k)] = 0, \quad (94)$$

$$\text{Var}(\xi_i(k)) = \frac{\|\mathbf{e}_k^T \mathbf{I}_0 \mathbf{Q}_i\|_2^2}{\text{SNR}_i}. \quad (95)$$

Re-casting $\mathbf{e}_k^T \mathbf{I}_0 \mathbf{Q}_i$ as a convolution of two vectors and using Young's convolution inequality, we achieve the following bound:

$$\text{Var}(\xi_i(k)) \leq \frac{1}{\text{SNR}_i}. \quad (96)$$

It follows that:

$$|\xi_i(k)| \leq \sqrt{\frac{2\log(\frac{1}{\varepsilon})}{\text{SNR}_i}},$$

with a probability of at least $1 - \varepsilon$. \square

APPENDIX E

LOCAL PERSPECTIVES FOR SIGNAL MODES DETECTION

To exploit the obscure multiplicative Vandermonde structure in (30), we could examine the following ratio between consecutive entries of $\tilde{\mathbf{Z}}_L^i$:

$$\hat{\mathbf{z}}_i(k) := \frac{\tilde{\mathbf{Z}}_L^i(k+1)}{\tilde{\mathbf{Z}}_L^i(k)} = \frac{z_i^k + \mathbf{E}_L^i(k+1)}{z_i^{k-1} + \mathbf{E}_L^i(k)}, \quad (97)$$

for $1 \leq k \leq N - L - 1$.

Informally, when $|\mathbf{E}_L^i(k)|$ and $|\mathbf{E}_L^i(k+1)|$ are sufficiently small, the ratio $\hat{\mathbf{z}}_i(k)$ in (97) can be approximated by:

$$\begin{aligned} \hat{\mathbf{z}}_i(k) &= \frac{z_i^k + \mathbf{E}_L^i(k+1)}{z_i^{k-1} + \mathbf{E}_L^i(k)} = z_i \left(\frac{1 + \frac{\mathbf{E}_L^i(k+1)}{z_i^k}}{1 + \frac{\mathbf{E}_L^i(k)}{z_i^{k-1}}} \right) \\ &\approx z_i \left(1 + \frac{\mathbf{E}_L^i(k+1)}{z_i^k} - \frac{\mathbf{E}_L^i(k)}{z_i^{k-1}} \right) \end{aligned} \quad (98)$$

using standard linear approximation techniques.

Equation (98) shows that the ratios between consecutive entries of the i -th signal mode are centered around a *constant* value, which is the i -th signal pole z_i . In the context of dynamic mode decomposition (DMD) for data-driven dynamical systems analysis, Bronstein et al. [7] proposed to use the features: $\epsilon_i = |\lambda_i - \mu_{\hat{\mathbf{z}}_i}|$, which can now be supported by the first-order approximation of λ_i , given by [5]:

$$\tilde{\lambda}_i \cong z_i + \frac{\mathbf{u}_i \mathbf{Q}_i \mathbf{w}}{b_i}.$$

APPENDIX F

ADDITIONAL NUMERICAL RESULTS

In this appendix, we provide the complementary results for Section VII. Fig. 9 is complementary for Fig. 6, and displays the average RMSE of the estimates $\{\hat{\theta}_i\}_{i=1}^M$ in dB versus the SNR. Fig. 10 is the same as Fig. 6, but displays the average RMSE of the estimates $\{\hat{\theta}_i\}_{i=1}^M$ and corresponding empirical bias in absolute value versus the number of samples N , for $M = 2$, $|\Delta\theta| = 2\pi/N$, and $\text{SNR}_{\text{dB}} = 8$. The complementary results for $M = 4$ shows high bias for the

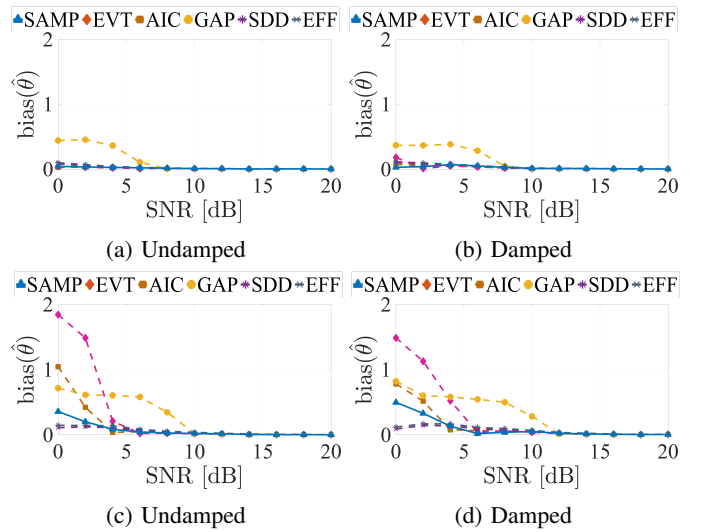


Fig. 9: Average bias in absolute value of $\{\hat{\theta}_i\}_{i=1}^M$ versus the SNR_{dB} , for $M = 2$ in (a)-(b), and $M = 4$ in (c)-(d).

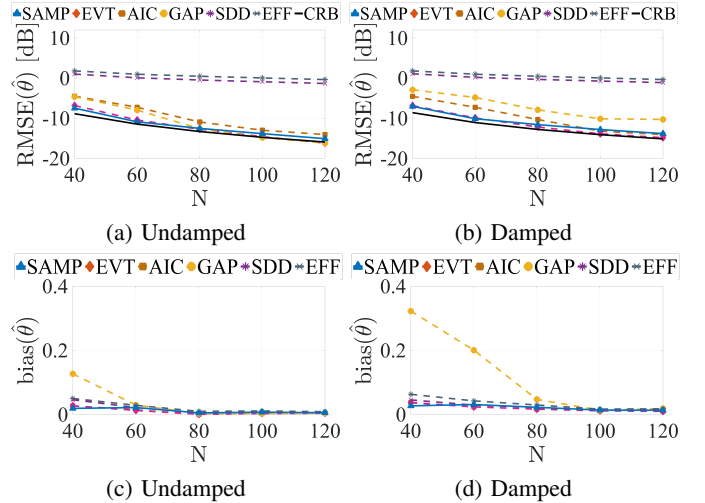


Fig. 10: Average RMSE and bias in absolute value of $\{\hat{\theta}_i\}_{i=1}^M$ versus the number of samples.

entire simulated range and are omitted. Fig. 11 is the same as Fig. 6, but displays the average RMSE of the estimates $\{\hat{\theta}_i\}_{i=1}^M$ and corresponding empirical bias in absolute value versus the frequencies separation, for $M = 2$, $N = 71$, and $\text{SNR}_{\text{dB}} = 10$. The complementary results for $M = 4$ shows high bias for the entire simulated range and are omitted.

REFERENCES

- [1] J. R. Magnus, "On differentiating eigenvalues and eigenvectors," *Econom. Theory*, vol. 1, no. 2, pp. 179–191, 1985.
- [2] A. Greenbaum, R.-c. Li, and M. L. Overton, "First-order perturbation theory for eigenvalues and eigenvectors," *SIAM Rev.*, vol. 62, no. 2, pp. 463–482, 2020.

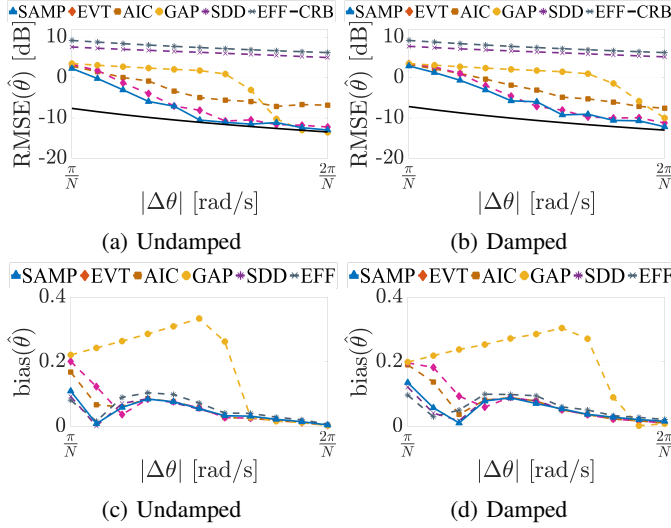


Fig. 11: Average RMSE and bias in absolute value of $\{\hat{\theta}_i\}_{i=1}^M$ versus the frequency separation.

- [3] A. Deif, “Rigorous perturbation bounds for eigenvalues and eigenvectors of a matrix,” *J. Comput. Appl. Math.*, vol. 57, no. 3, pp. 403–412, 1995.
- [4] G. Stewart, “Matrix perturbation theory,” *Computer Science and Scientific Computing/Academic Press, Inc*, 1990.
- [5] Y. Hua and T. K. Sarkar, “Matrix pencil method for estimating parameters of exponentially damped/undamped sinusoids in noise,” *IEEE Trans. Acoust. Speech Signal Process.*, vol. 38, no. 5, pp. 814–824, 1990.
- [6] P.-Å. Wedin, “Perturbation theory for pseudo-inverses,” *BIT Numer. Math.*, vol. 13, pp. 217–232, 1973.
- [7] E. Bronstein, A. Wiegner, D. Shilo, and R. Talmon, “The spatiotemporal coupling in delay-coordinates dynamic mode decomposition,” *Chaos: An Interdisciplinary Journal of Nonlinear Science*, vol. 32, no. 12, p. 123 127, 2022.